Herrero-Barbero Paula (Orcid ID: 0000-0002-2295-8338)
Martínez-Díaz José, J. (Orcid ID: 0000-0003-4846-0279)

Neogene basin inversion and recent slip rate distribution of the northern termination of the Alhama de Murcia Fault (Eastern Betic Shear Zone, SE Spain)

Paula Herrero-Barbero[1], José A. Álvarez-Gómez[1], José J. Martínez-Díaz[1,2] and Juan Klimowitz[3]

[1]Department of Geodynamics, Stratigraphy and Paleontology, Universidad Complutense de Madrid, Madrid, Spain.

[2]Instituto de Geociencias IGEO (UCM, CSIC), Madrid, Spain.

[3]GESSAL, Toronga, 26, Madrid, Spain

Corresponding author: Paula Herrero-Barbero (pherrerob@ucm.es)

Key Points:

- Seismic interpretation of a Neogene inverted basin bounded by the northern section of the Alhama de Murcia Fault.
- Long-term slip rate of 0.32 mm/yr (last 4.8-7.6 Ma) in the NE section, estimated from cross-section restoration and GPS motion vectors.
- Decrease of slip rate along the fault section and transference of deformation with other faults.

This article has been accepted for publication and undergone full peer review but has not been through the copyediting, typesetting, pagination and proofreading process which may lead to differences between this version and the Version of Record. Please cite this article as doi: 10.1029/2019TC005750

Abstract

The Alhama de Murcia Fault is one of the main active structures of the Eastern Betic Shear Zone (SE Spain), characterized by the presence, along its trace, of Neogene basins developed under Early to Late Miocene extensional tectonics. A dominant NNW-SSE shortening direction is active from Late Miocene driven by the present-day plate convergence. We present the structural analysis of the northeastern section of this fault, where reliable estimations of slip rates were unknown due to the lack of geomorphological evidence of recent activity. The recent tectonic evolution and reactivation of the northeastern section is closely related to the Fortuna basin development and tectonic inversion. We approach the structural analysis through the interpretation of seismic reflection profiles, well data, fieldwork and 3D geological modeling. We estimated a maximum long-term slip-rate of (0.32 +0.18/-0.13) mm/yr in the Librilla sector (last 4.8-7.6 Ma), based on cross-section restorations and assuming current motion trends from GPS data. According to the results from the cross-sections restored along the section and a vertical displacement analysis based on a 3D model, the slip-rate distribution shows a decrease of activity toward the northeastern tip of the studied fault section. This supports a transference of deformation between the Alhama de Murcia Fault and the Carrascoy Fault, which seems to absorb part of the shortening during the Plio-Quaternary, explaining the lower relief created by the activity of the northeastern section. The slip rates obtained have important implications in seismic hazard assessments and in the distribution of deformation along the region.

1 Introduction

Slip rate estimations on active faults are essential for our understanding of seismic potential and earthquake recurrence in a region (e.g., Youngs & Coppersmith, 1985). The quantification of slip rates shows certain degree of complexity in areas with low regional strain rates and moderate seismicity (Scholz & Cowie, 1990), such as the Eastern Betic Shear Zone (EBSZ, SE Iberian Peninsula; Figure 1a), the Betic branch of the Trans-Alboran Shear Zone (De Larouzière et al., 1988), where the deformation is distributed across an array of faults. Frequently, this context requires the obtaining of slip rates from multiple observations (e.g., geological, geomorphic and geodetic) over different timescales and using different techniques (Cowie et al., 2012).

The Alhama de Murcia fault (AMF; Figure 1), first described by Montenat (1973), is an 87-km N40ºE-N65ºE left-lateral strike-slip fault with reverse component (Bousquet, 1979; Martínez-Díaz, 1998) since, at least, Late Miocene (Montenat et al., 1987). Since that moment, the change of the regional stress field produced a compressional inversion of former extensional sedimentary basins bounded by the Alhama de Murcia fault (Martínez-Díaz, 1998; Montenat, 1973) and initiated the present-day transpressional behavior of the fault.

Most of the destructive historical earthquakes that have occurred along the Guadalentín Valley, including the 2011 Lorca earthquake (Martínez-Díaz et al., 2012a), as well as an important part of the instrumental seismicity, appear to be associated with the AMF; especially to the southern sections (Figure 1). The seismic potential of the northeastern sections should not be neglected. The historical seismic catalog (IGN, 2018) contains references to EMS VII-VIII earthquakes (Alhama de Murcia, 1855; Las Torres de Cotillas and Lorquí, 1911) and three EMS VI earthquakes (Alhama de Murcia 1864; Alcantarilla 1902 and 1905), spatially associated with the AMF (Figure 1a). The most remarkable instrumental earthquake near the northeastern section was recorded close to Alhama de Murcia in 1996 with a magnitude mbLg 3.5 (EMS III-IV). The need to improve our

knowledge about the seismic potential in the northern sector of the AMF is also justified by the proximity to the city of Murcia (Figure 1a), with a population of more than 400,000 inhabitants.

Obtaining net slip rates of this fault requires the estimation of both components of displacement, either directly or indirectly: the lateral slip rate and the vertical slip rate. The slip rates measurements of the AMF have been estimated so far through morphotectonic and paleoseismic studies, in many cases with great uncertainties associated (Ferrater et al., 2016, 2017; Ortuño et al., 2012; Martínez-Díaz et al., 2003; Masana et al., 2004). Martínez-Díaz (1998), Martínez-Díaz et al. (2003) and Ortuño et al. (2012) estimated lateral slip rates based on morphotectonic analysis of offset channels for the southern sections of the AMF (Góñar-Lorca and Lorca-Totana fault sections; Figure 1b). Estimations of all the components of the slip rate were calculated by Martínez-Díaz et al. (2003) and Masana et al. (2004) by means of paleoseismic trenching. They suggested a vertical slip rate of 0.04-0.35 mm/yr in the Lorca-Totana section and, using the orientation of slickensides on the fault plane observed in the trenches, estimated a 0.07-0.66 mm/yr net-slip rate for the last 30 kyr. Recently, a three-dimensional paleoseismic study in the same section (Ferrater et al., 2016) suggests a 0.9 ± 0.1 mm/yr net-slip rate for the last 20 kyr, which is a value significantly larger. Moreover, Ortuño et al. (2012) estimated a net slip rate of 0.16-0.24 mm/yr for the last 47-63 kyr based on several paleoseismic sites in the Góñar-Lorca section.

Therefore, most of the estimations of slip rates in the Alhama de Murcia fault have been obtained by some evidence located at the southwestern sections of the fault: Góñar-Lorca and Lorca-Totana (Figure 1b). In these sections the AMF is bounding prominent reliefs (Las Estancias and La Tercia ranges) and geomorphologic offset markers are numerous. According to the geometry of the fault zone, the morphological expression and the seismicity, Martínez-Díaz et al. (2012b) considered other two structural sections in the northeast side of the AMF (Figure 1b): Totana – Alhama de Murcia (N40ºE) and Alhama de Murcia – Alcantarilla (N45ºE). The former splits into two branches, one of them bounding the Espuña range (the Amarguillo Fault) with N20ºE strike, while the other trace continues partially covered by Quaternary alluvial fan deposits toward Alhama de Murcia town. The Alhama de Murcia – Alcantarilla section (N45ºE) (Figures 1b and 2), northeastern termination of the AMF, controlled the evolution of the Fortuna Basin on its hanging wall but shows low geomorphic expression. Martínez-Díaz (1998) suggested that the lower activity in this section may be related to a transfer of deformation to the Quaternary Carrascoy fault (Figure 1a), located only 5 km east of the Alhama de Murcia – Alcantarilla section.

The lack of geomorphological evidence showing recent activity in the Totana – Alhama de Murcia and Alhama de Murcia – Alcantarilla sections results in an absence of Quaternary slip rates estimated at the northern termination of the Alhama de Murcia fault. The only known slip rates derive from a geomorphological classification of mountain fronts (Silva et al., 2003), estimating an uplift rate of 0.03-0.07 mm/yr for the reliefs which are currently bounding the Quaternary Guadalentín depression (Figures 1b, 2).

Due to the absence of paleoseismic data in the northeastern sector of the AMF and the need to obtain seismic parameters to evaluate the seismic hazard in this area, the estimation of the slip rate should be approached from another perspective. The recent tectonic evolution of the AMF in this section is closely related to the Miocene Fortuna basin development and tectonic inversion. The structural features of this sedimentary basin, as well as the stratigraphic markers deformed by the fault movement, can be used to restore, using quantitative analysis of cross sections, the displacement owing to the transpressive reactivation of the AMF in Late Miocene.

Cross-section restoration was first presented in studies of compressional terranes (e.g., Bally et al., 1966; Dahlstrom, 1969; Mitra & Namson, 1989). Then, it was used in extensional areas (e.g., Davison, 1986; Gibbs, 1983; Groshong, 1989; White & Yielding, 1991) and also in inverted extensional basins (e.g., Bishop & Buchanan, 1995; Bulnes & McClay, 1998; Butler, 1989; Sibson & Ghisetti, 2010). The first 2D restorations were carried out by using the equal area method (Chamberlin, 1910), the line-length method (Dahlstrom, 1969) or a combination of both (Mitra & Namson, 1989). Lately, other 2D cross-section restoration methods such as trishear, flexural slip and fault-parallel flow techniques, have been developed considering the structural features of each tectonic regime (Allmendinger, 1998; Bulnes & McClay, 1999; Egan et al., 1997). These restoration techniques were implemented in computer programs that have allowed accurate cross-section restorations in active tectonics studies (e.g., Geiser et al., 1988; Lopez-Mir et al., 2014; Watkins et al., 2017).

In this work, the interpretation of seismic reflection profiles and well data from the Fortuna basin provides the structural features and markers needed to apply techniques of cross section restoration. The description of the interpreted structures leads to a better understanding of the tectonic framework of the area. We present a three-dimensional model showing the tectosedimentary relationship between the Fortuna basin architecture and the faults interpreted in the area. From the restorations, we estimate the resulting displacement following the transpressive reactivation of the Alhama de Murcia fault in Late Miocene. Finally, we analyze the slip-rate distribution along the Alhama de Murcia – Alcantarilla section. The rates estimated from the restoration of this research are long-term slip rates, considering a time interval since the Late Miocene – Pliocene.

2 Geological Setting

The Alhama de Murcia Fault is located in the Eastern Betic Shear Zone (EBSZ; Figure 1a), the Betic branch of the Trans-Alboran Shear Zone (De Larouzière et al., 1988). This area is composed of Paleozoic and Mesozoic rocks from Alpujárride and Maláguide tectonic complexes, in addition to several Neogene marine basins associated with two extensional phases occurred between Burdigalian and Tortonian (Martínez-Martínez & Azañón, 1997; Rodríguez-Fernández et al., 2012). After the extensional phases, a compressional stress field was established with a dominant NNW-SSE shortening direction driven by the convergence between the Eurasian and African plates since the Late Miocene (Sanz de Galdeano, 1990). The present-day rate of convergence is about 4-6 mm/yr (Argus et al., 1989; Nocquet, 2012; Serpelloni et al., 2007) and the EBSZ could be absorbing up to 31% of the shortening (Masana et al., 2004). Recently, geodetic analysis based on local GPS data have yielded a horizontal slip rate estimation of 1.5 ± 0.3 mm/yr (Echeverría et al., 2013) for the shear zone including the AMF and the Palomares fault (Figure 1a). This tectonic evolution from Miocene to Quaternary results in a 'basin and range' structure (Meijninger & Vissers, 2006; Montenat & Ott d'Estevou, 1999) made up of E-W to ENE-WSW mountain ranges (Las Estancias, La Tercia and Espuña ranges) separated by Neogene and Quaternary basins (Huercal Overa, Lorca and Fortuna basins).

The area of this study (Figure 2) is located at the southwestern sector of the Fortuna basin, in the region where the AMF is bounding the Miocene basin and the Guadalentín Quaternary depression. Some authors have traditionally referred to this sector as the Mula subbasin (Martínez del Olmo et al., 2010) or Archena-Mula sector (Loiseau et al., 1990). In this work, we will refer to this area as Mula-Archena subbasin.

2.1 Basin Stratigraphy

The Neogene sedimentary infill of the southwestern sector of the Fortuna basin, deposited after the exhumation of the tectonometamorphic complexes of the Alboran domain, is characterized by three successions: a Late Serravallian coarse-grained detrital unit deposited in a continental environment, a transgressive marine succession represented mostly by Tortonian marine marls, and a regressive transitional to continental succession that includes Messinian evaporite units and a thick continental alluvial and fluvial unit developed during Pliocene and Quaternary. Figure 3 shows a correlation between the lithostratigraphic units described below, the Murcia 4-1 well-log (IGME, 2018) and the stratigraphic formations described in the region.

The base of the basin sedimentary record (Units I and II; Figure 3) is represented by continental conglomerates formed by dolomite and schist clasts with a hardened reddish calcareous matrix, grading upwards into sandstones (Montenat et al., 1990). This succession have been correlated with the conglomerates and sandstones of the Relojero Fm. and Cresta del Gallo Fm., described as from Langhian-Serravallian age (Dabrio & Polo, 1991) in the Murcia basin. At the area near the Alhama de Murcia fault zone, these conglomerates have been observed close to the Alhama de Murcia town (Figure 2).

At the base of La Muela range (Figure 2), yellowish silty marls with gypsum are concordant with the red conglomerates described above. These sediments (Unit III; Figure 3) are covered by calcarenites, sandstones and hardened polymictic conglomerates at the top of the mountain range, progressively thinning toward Sierra Espuña. Both series and the continental red conglomerates constitute the oldest unit of the basin in this sector (Unit I, II and III), defined as Upper Serravallian to Lower Tortonian sediments (Booth-Rea et al., 2002) sealing the upper allochthonous units of the Alboran Crustal Domain.

Unconformably overlying the conglomerates succession, a thick deposit of gray marls, first described by Montenat (1973), represents the transgressive marine sequence in the basin (Unit IV; Figure 3). These marls are widely distributed at the north of the subbasin and migrate laterally into delta and reef facies toward the western and southeastern margins of the basin (Lonergan & Schreiber, 1993; Santisteban & Taberner, 1983). This marine unit was developed throughout the Tortonian and some studies suggested a Messinian age for the upper part of the succession (Müller and Hsü, 1987, Lukowski et al., 1988); whereas magnetostratigraphic studies from Krijgsman et al. (2000) suggest late Tortonian age at the top of the marls unit.

Overlying the Tortonian marls, a regressive sequence of gypsiferous marls, massive gypsum and detrital deposits is represented in the Fortuna basin (Unit V, Figure 3), having been distinguished up to four different evaporitic events (Dinares-Turrell et al., 1999; Krijgsman et al., 2000; Lukowski et al., 1988; Müller & Hsü, 1987; Playà et al., 2000; Santisteban & Taberner, 1983). At the SW edge of the Fortuna basin, in the Librilla area (Figure 2), Ortí et al. (1993), Playà et al. (2000) and Garcés et al. (2001) described three main evaporitic units (Librilla Gypsum, Chicamo Gypsum-Chicamo Cycles Fm. and Ribera Gypsum) with nodular-laminated gypsum lithofacies, marls and diatomites. The evaporites of the Fortuna basin have commonly been correlated with the Messinian Mediterranean Salinity Crisis (Dinares-Turell et al., 1999; Lukowski et al. 1988; Müller & Hsü, 1987). Nevertheless, several authors supported on the paleontological record, suggested that this basin shows an early restriction event before the main Messinian Salinity Crisis. That favored a Tortonian Salinity Crisis (7.6-7.8 Ma), proposed as the consequence of a tectonic uplift event isolating

the eastern Betic basins (Corbí et al., 2012; Garcés et al., 1998, 2001; Krijgsman et al., 2000; Lancis et al., 2010; Montenat et al., 1987; Tent-Maclús et al., 2008).

In addition, there are several outcrops of Miocene volcanic lamproitic rocks in the Fortuna basin. Available petrological, geochemical and geochronological data from the lamproites report an age between 6.2 and 7.7 Ma for this rocks (Bellon et al., 1983; Kuiper et al. 2006; Montenat et al., 1975), what implies a Late Tortonian – Early Messinian vulcanism in the Fortuna basin. This confined period of Late Miocene magmatic activity developed within the eastern Betics is represented by the Barqueros volcano in the study area (Figure 2; Fúster & Gastesi, 1967; Montenat et al. 1975).

Lastly, the evaporite formations grade upwards into a continental succession (Unit VI; Figure 3). At the Mula – Archena sub-basin, the greater thickness of continental deposits are exposed in the sector of Librilla, filling the syncline structure between the Alhama de Murcia and the Barqueros faults (Figure 2). This sequence is characterized by alluvial red silts and conglomerates alternating with minor channelled conglomerates and sandstones. Datable fossil mammals indicate a late Messinian - early Pliocene age for the upper alluvial record (Garcés et al., 1998).

2.2 Basin structure and fault geometry

The Fortuna basin is bounded at its northern and southern sides (Figure 1a) by the Crevillente and Alhama de Murcia faults, respectively. Traditionally, some authors have interpreted the Fortuna basin as a strike-slip-controlled basin (De Larouzière et al., 1988; Montenat et al., 1987; Montenat & Ott d'Estevou, 1999), where the sinistral behavior on the AMF was initiated in the Tortonian age, implying an approximately N-S-directed compression. Other authors (e.g., Augier, 2004; Garcia-Dueñas et al., 1992; Meijninger, 2006; Vissers et al., 1995) describe extensional structures that involve a NE-SW to N-S-directed extension. Meijninger (2006) proposes that the Fortuna basin, as well as Lorca and Huercal Overa basins, are truly extensional basins: the Alhama de Murcia fault acted as a normal fault during late Serravallian to late Tortonian sedimentation, accommodating the extension; later, it was reactivated as an oblique reverse fault since Messinian (Armijo, 1977; Meijninger, 2006) in response to the current compressional stress field in the Eastern Betics. Both hypothesis have been used to describe the southwestern sector of the Fortuna basin (Mula-Archena sector). Amores et al. (2001) and Martínez del Olmo et al. (2010) analyzed some seismic profiles (some of them have been reinterpreted in this work) and interpreted a listric extensional fault in the position of the AMF; while Montenat and Ott d'Estevou (1999) consider that the Lorca and Fortuna basins are extensional zones whose evolution is related to strike-slip faulting and describe an extensional "horse tail" structure related to the AMF at the termination of the strike-slip fault, bounding the Fortuna basin.

3 Structural interpretation of seismic data

3.1 Geological and seismic data set

We analyze 2-D seismic reflection profiles lines (Figure 4), data from 3 wells and structural data collected through fieldwork in the studied area. The seismic lines and well data were acquired by Chevron and Enadimsa between 1983 and 1987, and they are available from IGME (2018) (http://info.igme.es/SIGEOF/). A geological map of the study area (Figure 2) has been produced based on previous cartography and cross sections (IGME,

1972a, 1972b, 2004), the review of relevant publications (e.g., Martínez-Díaz, 1998; Martínez-Díaz et al., 2012b; Meijninger, 2006; Montenat et al., 1990) and fieldwork.

The seismic profiles cover an area of ~ 500 km^2 in the southewestern edge of the Fortuna basin (Figure 4a), in the Mula-Archena subbasin. Only the most representative profiles and their interpretations are presented in this work; the rest of seismic interpretation is available in the Supporting Information. The NW-SE oriented seismic lines are approximately perpendicular to the AMF; three of them crosses the fault zone and the Guadalentín depression. Other two NE-SW oriented lines are subparallel to the AMF trace and intersect the rest of the seismic lines, helping to better constrain the interpretation. The seismic data are displayed in two-way traveltime (TWT) with a maximum penetration of 3.5 s, although the data are usually excessively noisy for detailed interpretation below 2-2.5 s TWT.

The well data helped to better constrain the seismic interpretation (Figure 3). Three wells were used: Murcia 4-1, Mula 2 and Mula 4 (Figure 4a). The Murcia 4-1 well reached a total depth of 2169 m; a gamma-ray log (GR) and a sonic log (DT) were taken from this well (Figure 3). The Mula 2 and Mula 4 wells are shallower (1000 m and 1020 m, respectively) and a sedimentological study was carried out. The three boreholes were located in the northern half of the subbasin, with no data available near the Alhama de Murcia fault zone. However, the lithostratigraphic description of the record from the wells allowed us to correlate the horizons subsequently interpreted in the seismic reflection profiles. The Murcia 4-1 well logs and velocity survey have eased the time-to-depth conversion. We have applied a Time-Depth polynomial function obtained from Murcia 4-1 velocity survey, which has been subsequently constrained by the lithostratigraphy of the three wells. Seismic-well calibration and seismic interpretation were performed with the software Petrel (Schlumberger™). The interpretations are constrained by surface and well data, where available. Even though significant uncertainties remain in the interpretation of horizons and structures, and despite the poor data quality of some seismic profiles, the elements required for our objectives have been identified.

The most identifiable seismic facies are the Serravallian-Lower Tortonian calcarenites and conglomerates (Unit III) intersected by Murcia 4-1 well. They form a continuous, thick and strongly reflective package in contrast to the underlying and overlying marls. The transition between the Upper Tortonian marls (Unit IV) and the Messinian gypsiferous marls (Unit V) also shows good reflectivity, probably owing to the presence of evaporitic layers. The noisy packages with greater continuity within the unit of Messinian marls have been interpreted as evaporitic level markers, distinguishing two intermediate horizons (Intra-Messinian 1 and Intra-Messinian 2) in addition to the base of the sequence. Defining the age of the intra-Messinian units and the evaporitic events to which they belong, raises uncertainty according with recent studies focused on the onset of evaporitic confinement. We assume that the markers Intra-Messinian 1, Intra-Messinian 2 and the base of the Unit V would range between the Upper Tortonian and Upper Messinian (7.8 – 5.3 Ma) (Corbí et al., 2012; Krijgsman et al., 2000; Lancis et al., 2010; Tent-Maclús et al., 2008).

As a result of the depth conversion, it is concluded that the basin depocenter, located in the AMF hanging wall, increases northeastward along the fault section, with thicknesses of Miocene sediments between 2200 and 3700 metres. This means that, at least in the Mula-Archena subbasin, the sedimentary wedge reaches a Miocene thickness remarkably greater than the depocenters estimated in Lorca basin (<1000 m, Montenat, 1973), also bounded by the AMF and located southward. The thickest sequence interpreted in the subbasin are the Upper Tortonian unit (IV) and the Messinian unit (V). From the subsidence curves of

previous studies in the Betic intramontane basins (Augier, 2004; Cloetingh et al., 1992; Garcés et al., 2001; Meijninger, 2006) it is concluded that the basin formation began in the early Tortonian, in a rapid extensional stage. The Fortuna basin was in open connection with the Guadalentin depression to the south and the Prebetic zone to the north, favoring the accumulation of more than 1000 m of Tortonian marine marls (Garcés et al., 2001). This scenario agrees with the thick Tortonian sequence interpreted in the seismic reflection profiles, whose correlation is especially good thanks to the wells. Meijninger (2006), on the other hand, suggest an interval of tectonic quiescence between two stages of uplift; during this interval, predominantly Messinian, extensional deformation had completely ended and the evaporitic sequence was deposited. For the purposes of our research, determining which stage of uplift actually corresponds to the initiation of inversion of faults is a key issue. Meijninger (2006) considers that the reactivation occurred in the latest Messinian – earliest Pliocene stage; however other studies suggest an earlier late Tortonian – early Messinian age (Cloetingh et al., 1992) in other basins in the region.

In order to better visualize the geometry of the Mula-Archena subbasin and try to solve some of the issues previously mentioned, a three-dimensional model based on the seismic interpretation has been constructed (Figure 5). Surfaces have been created using the ordinary kriging algorithm as interpolation technique in 3D Move™ software (Midland Valley). The ordinary kriging algorithm calculates the statistical relationship (variance) between similarly spaced data points. Besides the top horizons of the interpreted units, point data also have been incorporated into the model, such as well markers and dip data. By constructing surfaces from parallel cross sections, the meshes were expected to reveal possible anisotropies that were sub-parallel to sections. We measured these directional variations and incorporated them in the kriging procedure to balance the sagging artifacts, in order to achieve the overall accuracy of the model.

3.2 Description of the interpreted structures

The major fault systems interpreted in the seismic reflection profiles are, from south to north (Figure 4a): Algezares-Casas Nuevas Fault (ACNF), Alhama de Murcia Fault (AMF), Barqueros Fault (BF) and Mula-Archena Fault. Besides these principal structures, there have been interpreted other minor faults in the Miocene basin and in the Guadalentin depression. Some of these minor faults present a quantifiable slip while others do not have sufficient resolution to estimate their displacement.

The Alhama de Murcia fault zone is shown in the seismic profiles as a set of diffractions that reveal an area of intense fracturing. It has been interpreted as a major fault that correlates with the trace mapped through fieldwork, aerial photographs and LiDAR-derived digital terrain models. In a broader tectonic context, the Alhama de Murcia fault zone forms part of an area of active oblique compressional inversion with a predominant NNW-SSE shortening regime. Within this area, normal faults inherited from Early Miocene extensional phase have undergone reverse and strike-slip reactivation since the Late Miocene – Pliocene (Meijninger & Vissers, 2006), even though the mechanics of the reactivation is still under discussion. The interpretation of the 2D seismic cross-sections shown in this work reveals some features that support that the AMF has experienced, indeed, a transpressional reactivation. Some of these features are neoformed structures, as a result of the adaptation of the reactivated faults to an optimal orientation within the compressive stress field. Overall, the seismic lines show uplifted anticline folds affecting the upper Miocene formations in the AMF hanging wall; in some cases, they represent incipient compressional inversion with

'harpoon-head' folding (McClay, 1995) of the syntectonic sequence (Figure 4b). The onlap and flexure of the interpreted intra-Messinian units above the Upper-Tortonian top sequence may represent progressive compressional reactivation during the Messinian, generating a growth anticline in the fault hanging wall. Besides, some profiles evidence a decrease of the fault dip at the surface (Figure 4c), possibly associated with a reverse-fault refracting to low-dip in the Pliocene cover sediments arising from compressional inversion (Sibson & Ghisetti, 2010).

Several NW-SE cross sections end at the base of the Plio-Quaternary alluvial fans located on the northern front of the Carrascoy Range (Figure 4a). At the southwest termination of the Carrascoy Range, a wide fault zone is bounded by two main faults: the Carrascoy Fault, a left-lateral strike-slip subvertical fault dipping southeastward and controlling the former mountain front (Sanz de Galdeano et al. 1998); and the Algezares-Casas Nuevas fault, a younger blind reverse fault dipping to the south (Martín-Banda et al., 2015) that accommodates broad propagation folds along the segment. The Algezares-Casas Nuevas fault has been interpreted in the seismic profiles whose data quality has allowed to identify possible diffractions associated with the mapped fault trace (IGME, 2019). In addition, several reverse SSE-dipping faults have been correlated along the Guadalentin depression (INV 1-4; Figure 4c), generating small offsets in the Plio-Messinian units. These faults may be related to the Quaternary activity of the Carrascoy Fault System, revealing that the compressive deformation was propagated to the NNW, in accordance with the development of a foreberg-style faulting with northward vergence as proposed by Martín-Banda et al. (2015).

Other relevant structure from our seismic interpretation is the Barqueros fault (Figure 2), a NNE-SSW antithetic fault, oblique to the AMF (IGME, 1972a; Montenat & d'Estevou, 1999), which seems to join with the AMF at depth into the basement. In a context of extension, the presence of an antithetic normal fault agrees with a typical collapse graben. Although the present-day finite displacement observed in the units III and IV and partially in unit V matches a normal fault, a compressional reactivation under the dominant stress field cannot be ruled out. In profile S-84-55 (Figure 4d), which obliquely crosses the Barqueros fault, a slight folding is observed in the hanging wall, maybe associated with a roll-over structure but also with syn-inversion strata. On the other hand, this fault is bounding, together with the AMF, a syncline developed on Plio-Quaternary continental sediments (Unit VI). In the wedge between the two faults, internal unconformities and closed folds with angular hinges are observed into the Pliocene materials cropped out (Figure 2). These materials seem to be syntectonic during the inversion of the structure, implying a recent deformation conditioned by the presence of the Barqueros fault.

4 Cross-Section Restoration

In order to evaluate the interpretation and analyze quantitatively the structural evolution, a 2D sequential restoration has been carried out applying algorithms to simulate the reversal of geological processes. The cross-section restoration has allowed to assess the structural evolution of the Mula-Archena subbasin and to quantify the shortening and dip-slip related to the AMF from Late Miocene. 2D restoration does not permit to evaluate the lateral slip component of the AMF and therefore other methods have been applied for this purpose.

The cross-section restoration has been carried out through the combination of two kinematic methods implemented as algorithms in the Move 2D modeling software. The Fault-Parallel Flow method (Egan et al., 1997, 1999) has been used for modeling hanging

wall deformation which occurs discretely between beds over the fault plane. In Fault-paralell flow method, horizon movement is 'layer parallel': particles within the hanging wall translate parallel to the fault surface along flow paths (Ziesch et al., 2014). This model does not consider an internal deformation throughout the hanging wall; in this work a discrete deformation has been assumed to quantify the dip-slip and the heave between the traces of the interpreted bedding surfaces. This scale-independent method is theoretically applicable to a large range of fault geometries (Brandes & Tanner, 2014), so it is compatible with a multiple-dipping fault like the Alhama de Murcia fault or the Barqueros fault. For those restorations that require adjusting the geometry of the hanging-wall sequence due to the presence of a previous fold, the Trishear method (Allmendinger, 1998; Erslev, 1991) has been used locally. The trishear method models ductile deformation in a triangular area that propagates from the fault tip. This model allows to combine several parameters that modify the geometry as an amount of slip is reproduced: the angle of the triangular zone, the distribution of the deformation along the zone and the propagation-to-slip ratio (P / T ratio) are the most important. The trishear kinematic model estimates the same amount of slip as the Fault Parallel Flow method, although it does allow modeling the fold-related structures. The combination of Fault-parallel flow and thishear models tries to get closer to natural deformation.

Among the seismic profiles interpreted, we have chosen 3 sections (S-84-52, S-84-92, and S-84-56) that are considered the most representative and whose interpretation has given much information about the basin evolution and the kinematics of the faults. The profiles S-84-52 (Figure 6) and S-84-92 (Figure 7) are in the sector close to Librilla and the profile S-84-56 (Figure 8) are in the sector close to Alcantarilla; therefore we will refer to these sectors (Figure 2) in order to simplify the explanations. For the profiles that reflect the interpretation of the Guadalentín depression sequence (Figures 4c, 6 and 7), the reverse faults (INV 1-4) associated with the recent activity of Carrascoy – Algezares – Casas Nuevas fault (Martín-Banda et al., 2015) have also been restored, following a sequencing in accordance with the westward propagation of the deformation from the Carrascoy fault zone. We measured offsets of (153 +255 / -103) m for the INV 1-4 reverse faults (Figure 4c), applying Zechar and Frankel (2009) probability functions.

In the Mula-Archena subbasin, we have considered that the Barqueros fault and the AMF could move simultaneously in a syn-tectonic sequence during Late Miocene. The possible connection between the Barqueros normal fault and the last volcanic episode of the Barqueros volcano, would indicate the presence of activity at least since the Late Tortonian – Messinian (6-8 Ma, Bellon et al., 1983; Kuiper et al., 2006; Montenat et al., 1975), also controlling the syncline with the greater thickness of Pliocene detrital sediments (Figure 2). In order to reproduce the interaction of both faults during the Tortonian-Messinian, the marker horizons have been restored in several stages whose displacements amounts are added later.

The Tortonian top stratigraphic horizon (Units IV-V) is considered a reliable marker to estimate the minimum slip on the fault plane after the reactivation of the AMF as a sinistral-reverse fault. We consider that the main reactivation of the AMF occurred, at least, since Late Tortonian (Krijgsman et al., 2000, 2006); therefore, this marker horizon is considered prior to basin margins uplift and has not accumulated excessive extensional displacement compared to underlying beds. On the contrary, the upper Messinian sequence (units Intra-Messinian 1 and Intra-Messinian 2) could be developed after the basin inversion, maybe as a syn-tectonic sedimentation on the uplift of the fault hanging-wall, hence the fault offset only reveals a part of the total displacement.

The results estimated from the balanced sections show the total offsets measured in the Unit IV base horizon in successive stages of sequential restoration (Figures 6 and 7), with the exception of the profile S-84-56 (Figure 8), whose total dip-slip refers to the intra-Messinian markers. In Table 1, the dip-slip and heave results estimated in each balanced section are shown. We consider an uncertainty of ±3.4 m for each measure, based on the sample interval of the seismic lines transformed into depth in meters. The restoration of the selected markers shows total dip-slips of 1227 m, 673 m and 162 m in the profiles S-84-52, S-85-92 and S-84-56, respectively (Table 1). The estimation of the heave, understood as the horizontal projection of the dip-slip, has also been obtained using Move^{TM} tools and is dependent on the fault geometry. The values of heave estimated are 597 m, 319 m and 92 m for the profiles S-84-52, S-85-92 and S-84-56, respectively (Table 1).

We emphasize that these results are equivalent to a minimum slip in the post-Tortonian period because it is not possible to quantify the total syn-extensional displacement of the Serravallian-Tortonian units before the transpressive reactivation. The Figure 6c shows an estimation of the expected offset at the top of the Unit III before the basin inversion based on the regional tilting interpreted toward the SSE. This estimation has allowed to approximate a value of uplift for the sector of 'La Muela' (see in Discussion), at the southwest of the Alhama de Murcia – Alcantarilla section (Figure 2).

5 3D vertical displacement analysis

We have also carried out a fault displacement analysis using the 3D model of the subbasin (Figure 5) and the 3D geometry of the AMF interpreted from the seismic profiles available. Specifically, the throw distribution resulting from the vertical displacement of the fault hanging wall has been measured using the same stratigraphic horizons as in the cross-section restoration and comparing their intersections with the fault plane. Although the principles of fault displacement analysis can be applied to structures accommodating any slip orientation, much of the previous research was performed on normal faults (e.g., Bull et al., 2006; Faure-Walker et al., 2009; Roberts & Michetti, 2004), rather than on reverse or oblique faults (e.g., Chamot-Rooke et al., 1993; Krishna et al., 2009; Litchfield, 2001). Moreover, it is common to use this methodology to evaluate the reactivation of normal faults to a different kinematics (e.g. reverse or oblique faults) using throw mapping (Baudon & Cartwright, 2008; Giba et al., 2012; Nixon et al., 2014). In this work, the vertical displacement analysis in 3D allows:

a. Assessing the displacement distribution in the northern sector of the AMF along the fault trace. The aim is extending the quantitative analysis of fault displacement to three dimensions and compare it with the results of the cross-section restorations.
b. Identifying the zones where the stratigraphic horizons record positive inversion as a result of the transpressive reactivation. In our work, positive values of vertical displacement concern the latter, and negative values imply low or even null slip, which has not been able to balance the dip separation resulting from deformation before reactivation.

The analysis of displacement distribution shows a decrease of vertical throw along the fault segment, toward the northeast (Figure 9). The Tortonian top horizon (unit IV) accumulates the greatest vertical displacement, while intra-Messinian markers show a throw of 400 - 500 meters lower in the Librilla sector. Northeastward, the throw difference among

stratigraphic markers is significantly reduced, until reaching negative values at 13 km horizontal distance along the fault trace. From that point, the apparent offsets change to normal-fault displacement, probably because the decrease of shortening toward the northeast has prevented the extensional structures from being inverted. A remarkable increase of vertical throw is observed in all markers analyzed at 6-11 km horizontal distance (Figure 9). This zone matches with an antiformal structure where Messinian marls and gypsum crop out (Unit V; Figure 2). In the seismic sections (Figure 4b) an intense tilting of the upper horizons has been interpreted in the fault hanging-wall, although the offsets are not as large as the observed at the southwestern end of the section.

6 Slip-Rate estimation

Regarding the 2D and 3D analysis of slip along the northeastern segment of the Alhama de Murcia fault, slip rates have been estimated (Tables 2 and 3) with the aim of evaluating the implications on seismic hazard. We assume that fault heave is a measure of the shortening associated with the seismic slip on this fault section. Despite this, the implication of possible internal aseismic deformation due to shortening will be discussed, since it is reflected in the existence of anticlinal and synclinal folds in the hanging wall of the fault.

The age of the beginning of the basin inversion is a matter of debate, although it would be dated in the Late Miocene – Pliocene, based on the geodynamic framework (e.g., Armijo, 1977; Martínez-Díaz, 1998; Meijninger & Vissers, 2006; Montenat et al., 1987). Local tectonic control for evaporite formation in the Fortuna basin has been used by several authors to argue the uplifting of basin margins, defining an age from Late Tortonian (7.6-7.8 Ma) (Krijgsman et al., 2006) to Early Pliocene (4.8 Ma) (Garcés et al., 2001). For the estimation of slip rates in the present research, the range of 7.6 – 4.8 Ma has been considered (Table 2). The age is the most representative uncertainty in our analysis, because the contribution of the measured displacement uncertainty (± 3.4 m) in the estimation of rates is almost insignificant, hence we only consider it in the estimation of dip-slip and shortening rates. We use the software from Zechar and Frankel (2009) to compute and report the slip rates, providing uncertainty models of each measurement estimated in our work. The probability distributions and data from the profiles are available as part of the Supporting Information. At the sector of Librilla, dip-slip rates range between (0.198 +0.054/-0.035) mm/yr for the profile S-84-52 and (0.109 +0.030/-0.019) mm/yr in the profile S-85-92, where the bounds correspond to a 95.45% confidence interval about the median (Table 2). At the Alcantarilla sector (profile S-84-56), the values are quite small: (0.026 +0.007/-0.005) mm/yr. Thus, the shortening rates estimated from the heave values follow the same trend as the dip-slip rates (Table 2): (0.096 +0.027/-0.017) mm/yr, (0.051 +0.014/-0.009) mm/yr and (0.015 +0.004/-0.003) mm/yr for the profiles S-84-52, S-85-92 and S-84-56, respectively, with the same confidence interval. The results reported with uncertainties about the median equivalent to the 68.27% confidence interval are shown in Table 2 and the probability distributions are provided in the Supporting Information.

Cross-section restoration do not solve the estimation of the slip along strike, which is a required parameter to obtain the net slip of this section of the AMF. As throughout the northeastern fault section no appropriate outcrop or geomorphic indicator has been found to quantify the lateral offset, directions of horizontal GPS motion vectors from the CuaTeNeo network (Echeverría et al., 2013) have been taken (Figure 1a), assuming that the interseismic displacement is representative of the movement produced since the NNW-SSE shortening

became dominant. Figure 10 shows the GPS velocity azimuths of PURI, MAJA, MONT and GANU from Echeverria et al. (2013) but subtracting the mean value of GPS vectors of ESPU and TERC (Figure 1a) in order to consider the NW hanging wall of the AMF as a reference frame. Thus, GPS motion azimuths are N358ºE (PURI), N007ºE (MAJA), N013ºE (MONT) and N033ºE (GANU). The regional GPS vectors can be decomposed into a vector parallel to the fault equivalent to the strike-slip, and an orthogonal vector that we assume corresponds to the shortening. The measurements of shortening obtained by means of balanced sections are extrapolated to a direction orthogonal to the fault, that is, the mean dip direction of the AMF plane. The angles between the mean dip direction (316.5º) and the orientations of the profiles S-84-52, S-85-96 and S-84-56 are 12.5º, 5.5º and 15.5º, respectively (Figure 10). A mean dip angle of 59º has been assumed for the fault plane in all cases, based on the fault dips from the profiles interpreted and considering only the upper part of the fault (from surface to the basement). The strike-slip results based on the decomposition of the GPS trends according to the slips obtained in the present work are shown in Table 3. By a simple comparison with Table 2, a dip-slip / strike-slip ratio of 0.86 is estimated in the Librilla sector, while the ratio in the Alcantarilla sector is slightly lower, 0.74.

The strike-slip rates obtained denote a high dispersion (Table 3) due to the different orientation of the velocity vectors recorded in the nearby stations. In the Figure 10, the rakes of the net-slip vectors obtained are projected in a stereoplot, evidencing the bias derived from the different azimuth registered in the GANU site. The rake angles estimated of the net-slip vector on the AMF plane are: 66ºNE (from PURI), 58ºNE (from MAJA), 53ºNE (from MONT) and 25º NE (from GANU). At the Librilla sector, we estimate a net-slip rate of (0.300 +0.195/-0.129) mm/yr in the profile S-84-52, and a net-slip rate of (0.163 +0.106/-0.070) mm/yr in the profile S-85-92, where the uncertainty about the median is equivalent to the 95.45% confidence interval (Table 3). At the Alcantarilla sector, the net-slip rate estimated is (0.046 +0.030/-0.020) mm/yr. The results for a 68.27% confidence interval are shown in Table 3. The higher uncertainty in the upper bound of the intervals evidences again the dispersion caused by the different GPS convergence directions registered in the region.

7 Discussion

The study of the northeastern termination of the Alhama de Murcia fault derives from the need to obtain long-term slip rates in an area generally considered as a fault section with hardly any quantifiable evidence of Quaternary tectonic activity (García-Mayordomo, 2005; Silva et al. 2003). The estimation of slip rates is complex where there are inversion structures involved, since the finite displacement across the structures may be low or opposite to the expected slips in the dominant stress field, showing a misleading evidence of inactivity (Sibson & Ghisetti, 2010).

Although some uncertainties remain in the interpretation of horizons and faults, and despite the poor quality of seismic data, the markers required for the slip restoration have been identified. Uncertainties derived from the resolution of the geophysical data (± 3.4 m) in each section have been incorporated into the results obtained through the restorations. The limitations of the algorithms used to reproduce the kinematic mechanisms have been solved by combining several methods, producing a structurally consistent resultant deformation. The Fault-parallel flow method assumes a volume conservation in the hanging wall between deformed and restored states (Egan et al., 1997), although the bed length is not preserved in some cases (Ziesch et al., 2014). In the cross-sections of this work, very low values of line

elongation have been calculated (e<0.02), hence we assume that the effect of the fault geometry on the line length of the bedding surfaces and on the quantification of slip rates is negligible. Still, we do not ignore the implication of potential internal deformation due to shortening, which could be reflected in the existence of anticlines and synclines in the AMF hanging wall if they were produced by buckling, although fault-related passive folding cannot be ruled out. Folding is especially significant in the sector of Librilla, affecting the Messinian and Plio-Quaternary detrital materials (Unit VI) (Figure 2); unfortunately, seismic data do not have enough resolution in shallow depths to interpret them. The obtained heave is directly related to the shortening component of the fault slip; therefore, the results presented here do not consider the effect of any internal deformation and consequently it must be considered as a minimum shortening.

For the estimation of slip rates, we have defined a time interval for the last 7.6 – 4.8 Ma, based on the changes in the configuration of the Fortuna basin and the tectonic control for evaporite events (Garcés et al., 2001; Krijgsman et al., 2006; Meijninger, 2006). The seismic interpretation also reflects some Intra-Messinian markers which onlap slightly the emerged top Tortonian unit (Figures 4c and 7a), revealing that reverse slip could be already active during the Messinian or the Late Tortonian. Thus, we suggest that the most likely slip rates would be closer to those calculated for an age of tectonic reactivation of 7.6 Ma.

7.1 Implications of the seismic interpretation in the fault geometry

The interpretation of the AMF in the seismic profiles reveals that the mean orientation of the fault plane estimated in the Alhama de Murcia – Alcantarilla section is N 46º E – 59º NW (Figure 5), considering the upper part of the fault plane, until it penetrates into the basement. This main dip is obtained based on the dips estimated in the profiles S-84-52, S-85-92 and S-84-56 (56.9º mean dip in the analysis of the 3D fault plane). The mean dip is consistent with the preferred model of fault plane rupture (55º dip) obtained using InSAR data for the M_W 5.2 2011 Lorca earthquake (Martínez-Díaz et al., 2012a). During compressional inversion, normal faults are frequently reactivated as reverse faults, with present-day dip angles of 45º-60º (Sibson, 2009). The interpretation of a model of fault geometry in the present work brings evidence of the presence of inherited extensional structures. The dip angles interpreted here and the existence of some structures associated with a localized compressional inversion (Figure 4), can be explained by a transpressive reactivation of normal faults in the Late Miocene.

Into the Betic basement the interpretation of the fault is uncertain, since the quality of data is very poor below 2 s TWT (around 4 km). This requires, not only to consider moderate uncertainties in the interpretation of the structures, but also to propose scenarios that explain the possible geometries of the fault at depth and its interaction with the basement. There are several strong reflectors that some authors have interpreted as a low-angle normal fault separating the basement from the basin infill (Amores et al., 2001; Martínez del Olmo et al., 2010; Rodriguez-Fernández et al., 2012), being part of a detachment system dipping toward the NNW (Booth-Rea et al., 2002, 2004). We have correlated these strong reflectors between the seismic profiles and highlighted them with a dashed line in the interpretation (Figures 4b, 4c and 4d); although there is not enough quality information for concluding that this surface is part of a listric fault or a growth fault later reactivated, as Meijninger and Vissers (2006) suggested. Furthermore, other minor basement-penetrating faults have been interpreted in this work (Figures 4b, 4c and 4d); both synthetic and antithetic normal faults mostly affect the units II and III of the Lower-Middle Miocene. We highlight a set of synthetic faults

interpreted in the Alhama de Murcia fault footwall (Figures 4b and 4c). Despite their normal finite displacement, these faults may have been reactivated, forming together with the main Alhama de Murcia fault, a kind of "domino" system of possible inherited normal faults (McClay, 1989, 1995).

We suggest the presence of a system of steep normal faults that mainly affects the Lower Miocene units and the carbonate basement, accommodated by a main extensional detachment. The reverse component of the displacement in the AMF can be explained by the reactivation of a large normal fault, which would explain the formation of an accommodation zone and the extensional structures interpreted. This configuration is common in multiple worldwide examples of inverted basins (e.g., Bishop and Buchanan, 1995; Bulnes and McClay, 1998; Butler, 1989) and experimental models (Bonini et al., 2012). However, we should consider that the mechanism of transpressional reactivation of an inherited normal fault does not work in the same way by absorbing the shortening as by accommodating the strike-slip deformation. The optimal orientation of the fault plane in the stress field significantly influences the mechanism of transpressive reactivation (e.g., Alonso-Henar et al., 2015; Dooley & Schreurs, 2012; Rotevatn & Peacock, 2018). Strike-slip reactivation of major normal faults is only favored by low angles between the shortening direction and the fault (Del Ventisette et al., 2006), that is low angles of rake. The way to accommodate the strike-slip deformation in the northern end of the AMF cannot be described from seismic reflection data and the rakes estimated are not low enough, except for the rake from GANU GPS site. In addition, the available seismic sections do not allow to interpret if the AMF deepens as a planar fault below 3 kilometers. We cannot rule out that the system of inherited steep normal faults, interpreted in the seismic reflection profiles, has accommodated the strike-slip kinematics at a greater depth, instead of an inherited low-angle normal fault. The seismotectonic characterization of the crust from García-Mayordomo (2005) suggests a maximum depth of 12 km for the brittle zone; thus the propagation of the coseismic rupture of the AMF is still possible at a greater depth, also involving a deeper fault and enabling the displacement. The integration of slip rates estimated in this work and several scenarios of fault geometry into numerical models through computational simulations may help to evaluate the latter issues in further research.

7.2 Comparison of the results obtained with geological and geodetic data

The cross-section restorations have allowed to estimate a range of dip-slip and shortening rates associated with the Alhama de Murcia – Alcantarilla section of the AMF. However, in order to obtain the total slip rate of this segment, local geodetic data has been used. In the stereoplot of Figure 10, triangles represent the local convergence vectors from PURI, MAJA, MONT and GANU geodetic sites, considering the northern block of the AMF as the reference frame and subtracting a mean value of the GPS sites of ESPU and TERC (Figure 1a), located at the northern block. These orientations have been combined with the values and orientations of shortening and dip-slip estimated in our work to obtain the strike-slip and net-slip vectors for the northern termination of the AMF. The circles of the stereoplot (Figure 10) represent the rake angles on the fault plane (in red) of the resulted net-slip vectors. Obviously, the rakes show the same dispersion of orientations as the local convergence vectors. In order to distinguish the best-fit results, we compare them with seismological and geological data, represented in the stereoplot (Figure 10) in two ways: the blue circle represents the slip vector of the focal mechanism for the M_W 5.2 Lorca earthquake in 2011 (Lopez-Comino et al., 2012); the stars represent the extreme obliquity angles of simple shear direction suggested by Alonso-Henar et al. (2020) from the kinematic analysis

of the fault gouge from the shear zone in the Lorca-Totana section. Our results evidence a remarkable difference between the slip vectors obtained from PURI, MAJA and MONT geodetic sites (66ºNE, 58ºNE and 53ºNE, respectively) and the slip vector obtained using the GANU orientation (25ºNE); however, the GANU site is the nearest to the northern end of the AMF and the rake from the Lorca earthquake mechanism (44º on a N240ºE – 54º plane) is closer to the rake angle obtained from the GANU velocity vector. Furthermore, Alonso-Henar et al. (2020) propose a range of angles between 26º and 55º for the simple shear direction in a model of triclinic transpression. The angles of 25ºNE, 53ºNE and 58ºNE obtained from GANU, MONT and MAJA sites respectively in our research, are the rake values that best fit the model proposed by Alonso-Henar et al. (2020) in the AMF. Including the results from GANU site in the global kinematic results implies more influence of strike-slip movement and, therefore, a greater value of net-slip.

7.3 Slip – rate distribution

The estimations carried out in this work using cross-section restorations and 3D analysis of vertical displacement, evidence higher slip rates than the estimated before in the northeastern termination of the AMF (Figure 1b). From the vertical displacement analysis, we estimate an interval of uplift rate between 0.14-0.22 mm/yr (last 7.6-4.8 Ma) for the maximum throw in the Librilla sector, being higher values than the vertical slip rate of 0.07 mm/yr proposed by Silva et al. (2003) and Martínez-Díaz et al. (2012b) for the Alhama – Alcantarilla section. The analysis has been done from the Librilla sector to the northeast, where seismic information is available; although the prominent uplift of the 'La Muela' range (Figure 2), formed by Lower Tortonian-Serravallian rigid materials (Unit III), could evidence a greater throw than the observations in the S-84-52 profile. A simple extrapolation from the Unit-III tridimensional surface before the basin inversion (Figure 7c) toward the southwest, compared to the current topographic surface of the 'La Muela' range, shows a minimum vertical throw of 1161 m and a maximum of 2001 m without considering the erosion. This estimation translates into a maximum uplift rate of 0.26-0.42 mm/yr for the last 7.6-4.8 Ma in the sector of 'La Muela'.

From cross-section restoration and geodetic data available, we also analyzed the horizontal slip in Alhama – Alcantarilla section and therefore we propose a range of net slip rates. The restoration of specific marker horizons in the profiles S-84-52 and S-85-92 has allowed to characterize the slip rate for the sector of Librilla, at the middle of the section. The profile S-84-56 has allowed to quantify the slip rate at the Alcantarilla sector, toward the tip of the fault section. At 'La Muela' sector, there are no seismic profiles available to restore. Assuming the best-fit orientations of the slip vector, we estimated net-slip rates for the northern sector of the AMF defining a preferred range of net-slip values (Table 4), corresponding to MAJA, MONT and GANU, and an absolute minimum and maximum net-slip that includes all the GPS sites. As a result, we obtained a net-slip rate of (0.323 +0.178/-0.128) mm/yr and (0.176 +0.097/-0.070) mm/yr for the profiles S-84-52 and S-85-92, respectively, both located at the Librilla sector (Figure 4a). At the Alcantarilla sector, we estimated a net-slip rate of (0.049 +0.027/-0.019) mm/yr, corresponding to the profile S-84-56. In all cases, the range of ages is for the last 4.8-7.6 Ma and the uncertainty describes the 95.45% confidence interval about the median. The results for a 68.27% confidence interval are shown in Table 4. In Figure 11, we show the probability distribution of the results estimated according to the preferred orientation of the convergence vectors. Based on the observations of seismic reflection profiles, we suggest that some bounding discontinuities in the depositional sequence could evidence that the uplift was already active since the

Messinian. The Table 5 represents the rates and uncertainties for a range of ages between the last 7.6 Ma (Late Tortonian) and 5.3 Ma (end of Messinian).

The slip distribution along the studied sector denotes a decrease of activity from the southwest to the northeast, regarding the long-term slip rates. The vertical slip rate estimated for 'La Muela' sector evidences that the total slip rate could be even higher from Librilla toward the southwest. The net slip decrease from the sector of 'La Muela' to the northeastern end of the fault may be due to two reasons or a combination of both: on the one hand, faults generally show a gradual decrease in displacement toward the tip-line (Walsh and Watterson, 1989); on the other hand, the sector of Librilla would behave like a zone of transference. This scenario would explain a transference of the deformation between the Alhama de Murcia fault and other nearby fault systems, such as the Carrascoy fault and the Bajo-Segura faults, which are absorbing part of NNW-SSE shortening component during the Pliocene-Quaternary (Borque et al. 2019; Martínez-Díaz et al., 2012b). This would explain the decrease in the relief toward the northeast of the fault section.

At the Lorca – Totana section (Figure 1b), a 0.9 ± 0.1 mm/yr net slip rate is estimated recently (Ferrater et al., 2016). Thus, the slip rate is higher in Lorca – Totana section and seem to decrease toward the northern termination of the AMF. The estimation of long-term slip rates at the Totana – Alhama segment (Figure 1b) would help to test this hypothesis. The decrease of slip rate toward the northern termination of the AMF could replicate the same behavior observed in the southern end of the fault. This observation entails, however, some difficulties to consider in order to compare these different sets of data:

- First, the results estimated in the present research are long-term slip rates for the last 7.6 – 4.8 Ma. The slip rates in other sections of the AMF (Figure 1b) are calculated with more recent time spans, therefore the comparison with our results should be made cautiously. For example, at the Goñar – Lorca section (Figure 1b), Ortuño et al. (2012) estimate a net slip rate of 0.16 – 0.24 mm/yr, similar to the values obtained in Alhama – Alcantarilla section, whereas Ferrater et al. (2017) calculate 1.6 – 1.7 mm/yr strike-slip rate for the last 200 kyr, using a different methodology. The latter are similar to those obtained by GPS (1.5 ± 0.3 mm/yr; Echeverría et al., 2013) but for the whole EBSZ including the southern sections of the AMF and the Palomares fault (Figure 1).

- The long-term slip rate calculated for the northern section of the AMF is related with the unique branch interpreted at the Librilla and Alcantarilla sectors (Martínez-Díaz et al., 2012b), whereas in other segments of the fault the deformation is distributed among several branches. The rates estimated so far in the Lorca-Totana section from paleoseismological data are only from one of the three main branches (Masana et al., 2004; Ferrater et al., 2016).

- To obtain the results of this work, we used an assumption of constant long-term slip rate during the time period considered (last 7.6 – 4.8 Ma). Although this assumption is used commonly when calculating long-term neotectonic slip rates, we should be careful when dealing with possible changes in the activity of the AMF during that period. In the Carrascoy fault system, changes of activity in the Quaternary have been described (Martín-Banda et al. 2015), which would have implications in the transference of deformation between both faults and in the relief. Regional geodynamic changes as the proposed rotation of Nubia-Eurasia convergence (Calais et al., 2003; Reilinger & McClusky, 2011) could also explain variations of slip rates in the AMF during the Quaternary.

8 Conclusions

We used seismic interpretation, 3D vertical displacement analysis, cross-section restoration and GPS data for estimating long-term slip rates in the northern termination of the Alhama de Murcia Fault (Eastern Betic Shear Zone, SE Spain), where the lack of geomorphological evidence showing recent activity originates an absence of slip data and geometrical parameters estimated so far. We obtained dip-slip and shortening rates applying kinematic methods of restoration in several cross-sections along the fault trace; these values were combined with GPS motion vectors to estimate the strike-slip rates (Table 5). We estimated a maximum net-slip rate of (0.32 +0.18/-0.13) mm/yr in the southwestern sector of the fault section, and a minimum net-slip rate of (0.05 +0.03/-0.02) mm/yr in the northeastern sector (last 4.8-7.6 Ma), using a preferred range of GPS convergence vectors. The results show a northeastward decrease of slip rate toward the fault tip. Moreover, this slip-rate distribution along the northern section of the fault supports the hypothesis of transference of deformation between the Alhama de Murcia Fault and, at least, the nearby Carrascoy Fault system, which is absorbing part of the NNW-SSE shortening component during the Plio-Quaternary.

The recent tectonic evolution of the Alhama de Murcia fault in this section is closely related to the Miocene Fortuna basin development and inversion. A transpressive reactivation of the fault in Late Miocene could explain the dip of the fault plane interpreted (~ 59º) and some structural features associated with localized inversion observed from surface and subsurface data analyzed in the basin, with implications in the proposed models of fault geometry and basin evolution:

- The analysis of the seismic interpretation helps to constrain a preferred range of ages between Late Tortonian and Messinian for the transpressive reactivation of the Alhama de Murcia Fault.

- The poor quality of seismic data below the Betic basement makes it difficult to conclude the presence of a low-angle normal fault separating the basement from the basin infill, which would explain, however, the formation of an accommodation zone and some typically inverted structures observed. Furthermore, we suggest the presence of a system of inherited basement-penetrating steep faults, related to the Alhama de Murcia fault zone, that could accommodate the displacement at greater depth and also facilitate the reactivation of the fault with the recent kinematics.

- Although the transpressive reactivation seems evident, with our data we cannot rule out or support if the basin was developed as a truly extensional basin controlled by a large normal fault or if the conjugate strike-slip faulting controlled the formation of the basin. Further work is needed to resolve the role of the Alhama de Murcia Fault in the Miocene evolution of the Fortuna basin.

Long-term slip rates (Table 5) and geometrical features of the northern termination of the Alhama de Murcia Fault (Alhama de Murcia – Alcantarilla section) estimated in this research are essential for future assessments with implications to seismic hazard, paying particular attention to the proximity of the city of Murcia and to the linkages with other faults or sections of the Alhama de Murcia Fault.

Acknowledgements

This research has been supported by the project QUAKESTEP (CGL2017-83931-C3-1-P) and P. Herrero-Barbero work has been supported by a FPU grant, both funded by the

Spanish Ministry of Science and Innovation. Dataset for this research is available in this in-text data citation reference: IGME (2018) - Geophysical Information System of the Spanish Geological Survey (http://info.igme.es/SIGEOF/) with specific public license conditions available at http://info.igme.es/SIGEOF/doc/LICENCIA_USO_IGME_EN.pdf . The software MOVE 2018.2 was provided by Petroleum Experts Ltd. through the donation of an Academic License to the Department of Geodynamics, Stratigraphy and Paleontology of the Universidad Complutense de Madrid. We thank the GESSAL company for providing the licence of Petrel (Schlumberger™) and for their support in the seismic interpretation, and Jorge Alonso-Henar and José Luis Sánchez (UCM) for their support in the fieldwork. The authors greatly appreciate the constructive comments of Ramon Arrowsmith and an anonymous reviewer, which significantly helped to improve this paper.

References

Allmendinger, R. W. (1998). Inverse and forward numerical modeling of trishear fault-propagation folds. *Tectonics, 17*(4), 640-656. https://doi.org/10.1029/98TC01907

Alonso-Henar, J., Fernández, C., & Martínez-Díaz, J. J. (2020). Application of the analytic model of general triclinic transpression with oblique extrusion to an active deformation zone: The Alhama de Murcia Fault (SE Iberian Peninsula). *Journal of Structural Geology, 130*, 103924. https://doi.org/10.1016/j.jsg.2019.103924

Alonso-Henar, J., Schreurs, G., Martinez-Díaz, J. J., Álvarez-Gómez, J. A., & Villamor, P. (2015). Neotectonic development of the El Salvador Fault Zone and implications for deformation in the Central America Volcanic Arc: Insights from 4-D analog modeling experiments: Neotectonic development of the ESFZ. *Tectonics, 34*(1), 133-151. https://doi.org/10.1002/2014TC003723

Amores, L. R., Hernández-Enrile, J. L. & Martínez-Díaz, J. J. (2001). Sobre los factores relacionados con la evaluación de la peligrosidad sísmica en la región de Murcia. *Segundo Congreso Iberoamericano de Ingeniería Sísmica*. Asociación Española de Ingeniería Sísmica, Madrid, Spain.

Argus, D. F., Gordon, R. G., DeMets, C., & Stein, S. (1989). Closure of the Africa-Eurasia-North America Plate motion circuit and tectonics of the Gloria Fault. *Journal of Geophysical Research: Solid Earth, 94*(B5), 5585-5602. https://doi.org/10.1029/JB094iB05p05585

Armijo, R. (1977). *La zone de failles de Lorca-Totana (Cordilleres Betiques, Espagne) etude tectonique et neotectonique* (Doctoral dissertation) Univ. Paris VII, Paris.

Augier, R. (2004). *Evolution tardi-orogenique des Cordilleres Betiques (Espagne): apports d'une etude integree* (Doctoral dissertation). Université Pierre et Marie Curie-Paris VI.

Bally, A. W., Gordy, P. L., & Stewart, G. A. (1966). Structure, Seismic Data, and Orogenic Evolution of Southern Canadian Rocky Mountains. *Bulletin of Canadian Petroleum Geology, 14*(3), 337-381.

Baudon, C., & Cartwright, J. (2008). The kinematics of reactivation of normal faults using high resolution throw mapping. *Journal of Structural Geology, 30*(8), 1072-1084. https://doi.org/10.1016/j.jsg.2008.04.008

Bellon, H., Bordet, P. & Montenat, C. (1983). Chronologie du magmatisme neogene des Cordilleres Betiques (Espagne meridionale). *Bulletin de La Societe Geologique de France, S7-XXV*(2), 205-217. https://doi.org/10.2113/gssgfbull.S7-XXV.2.205

Bishop, D. J., & Buchanan, P. G. (1995). Development of structurally inverted basins: a case study from the West Coast, South Island, New Zealand. *Geological Society, London, Special Publications, 88*(1), 549-585. https://doi.org/10.1144/GSL.SP.1995.088.01.28

Bonini, M., Sani, F., & Antonielli, B. (2012). Basin inversion and contractional reactivation of inherited normal faults: A review based on previous and new experimental models. *Tectonophysics, 522-523*, 55-88. https://doi.org/10.1016/j.tecto.2011.11.014

Booth-Rea, G., Azañón, J. M., & García-Dueñas, V. (2004). Extensional tectonics in the northeastern Betics (SE Spain): case study of extension in a multilayered upper crust with contrasting rheologies. *Journal of Structural Geology, 26*(11), 2039-2058. https://doi.org/10.1016/j.jsg.2004.04.005

Booth-Rea, G., García-Dueñas, V., & Azañón, J. M. (2002). Extensional attenuation of the Malaguide and Alpujarride thrust sheets in a segment of the Alboran basin folded during the Tortonian (Lorca area, Eastern Betics). *Comptes Rendus Geoscience, 334*(8), 557-563. https://doi.org/10.1016/S1631-0713(02)01794-7

Borque, M. J., Sánchez-Alzola, A., Martin-Rojas, I., Alfaro, P., Molina, S., Rosa-Cintas, S., ... & Herrera-Olmo, A. (2019). How Much Nubia-Eurasia Convergence Is Accommodated by the NE End of the Eastern Betic Shear Zone (SE Spain)? Constraints From GPS Velocities. *Tectonics, 38*(5), 1824-1839. https://doi.org/10.1029/2018TC004970

Bousquet, J.C. (1979). Quaternary Strike-Slip Faults in Southeastern Spain. In C.A. Whitten, R. Green and B.K. Meade (Eds.), *Developments in Geotectonics* (Vol. 13, pp. 277-286). https://doi.org/10.1016/B978-0-444-41783-1.50044-1

Brandes, C. & Tanner, D. C. (2014). Fault-related folding: A review of kinematic models and their application. *Earth-Science Reviews, 138*, 352-370. https://doi.org/10.1016/j.earscirev.2014.06.008

Bull, J. M., Barnes, P. M., Lamarche, G., Sanderson, D. J., Cowie, P. A., Taylor, S. K., & Dix, J. K. (2006). High-resolution record of displacement accumulation on an active normal fault: implications for models of slip accumulation during repeated earthquakes. *Journal of Structural Geology, 28*(7), 1146-1166. https://doi.org/10.1016/j.jsg.2006.03.006

Bulnes, M., & McClay, K. (1999). Benefits and limitations of different 2D algorithms used in cross-section restoration of inverted extensional faults: application to physical experiments. *Tectonophysics, 312*(2-4), 175-189. https://doi.org/10.1016/S0040-1951(99)00161-4

Bulnes, M., & McClay, K. R. (1998). Structural analysis and kinematic evolution of the inverted central South Celtic Sea Basin. *Marine and Petroleum Geology, 15*(7), 667-687. https://doi.org/10.1016/S0264-8172(98)00029-4

Butler, R. W. H. (1989). The influence of pre-existing basin structure on thrust system evolution in the Western Alps. *Geological Society, London, Special Publications, 44*(1), 105-122. https://doi.org/10.1144/GSL.SP.1989.044.01.07

Calais, E., DeMets, C., & Nocquet, J. M. (2003). Evidence for a post-3.16-Ma change in Nubia–Eurasia–North America plate motions?. *Earth and Planetary Science Letters, 216*(1-2), 81-92.

Chamberlin, R. T. (1910). The Appalachian Folds of Central Pennsylvania. *The Journal of Geology, 18*(3), 228-251. https://doi.org/10.1086/621722

Chamot-Rooke, N., Jestin, F., & Voogd, B. de. (1993). Intraplate shortening in the central Indian Ocean determined from a 2100-km-long north-south deep seismic reflection profile. *Geology, 21*(11), 1043. https://doi.org/10.1130/0091-7613(1993)021<1043:ISITCI>2.3.CO;2

Cloetingh, S., van der Beek, P. A., van Rees, D., Roep, T. B., Biermann, C., & Stephenson, R. A. (1992). Flexural interaction and the dynamics of neogene extensional Basin formation in the Alboran-Betic region. *Geo-Marine Letters, 12*(2-3), 66-75. https://doi.org/10.1007/BF02084914

Corbí, H., Lancis, C., García-García, F., Pina, J. A., Soria, J. M., Tent-Manclús, J. E., & Viseras, C. (2012). Updating the marine biostratigraphy of the Granada Basin (central Betic Cordillera). Insight for the Late Miocene palaeogeographic evolution of the Atlantic–Mediterranean seaway. *Geobios, 45*(3), 249-263.

Cowie, P. A., Roberts, G. P., Bull, J. M., & Visini, F. (2012). Relationships between fault geometry, slip rate variability and earthquake recurrence in extensional settings: Fault geometry control on earthquake rupture. *Geophysical Journal International, 189*(1), 143-160. https://doi.org/10.1111/j.1365-246X.2012.05378.x

Dabrio, C. J. & Polo, M. D. (1991). Fan-delta slope deposits and sequences in the Murcia-Carrascoy Basin (Late Neogene, SE. Spain). *Cuadernos de Geología Ibérica, 15*, 49-71.

Dahlstrom, C. D. A. (1969). Balanced cross sections. *Canadian Journal of Earth Sciences, 6*(4), 743-757. https://doi.org/10.1139/e69-069

Davison, I. (1986). Listric normal fault profiles: calculation using bed-length balance and fault displacement. *Journal of Structural Geology, 8*(2), 209-210. https://doi.org/10.1016/0191-8141(86)90112-4

De Larouzière, F. D., Bolze, J., Bordet, P., Hernandez, J., Montenat, C., & Ott d'Estevou, P. (1988). The Betic segment of the lithospheric Trans-Alboran shear zone during the Late Miocene. *Tectonophysics, 152*(1-2), 41-52. https://doi.org/10.1016/0040-1951(88)90028-5

Del Ventisette, C., Montanari, D., Sani, F., & Bonini, M. (2006). Basin inversion and fault reactivation in laboratory experiments. *Journal of Structural Geology, 28*(11), 2067-2083. https://doi.org/10.1016/j.jsg.2006.07.012

Dinarès-Turell, J., Ortí, F., Playà, E., & Rosell, L. (1999). Palaeomagnetic chronology of the evaporitic sedimentation in the Neogene Fortuna Basin (SE Spain): early restriction preceding the `Messinian Salinity Crisis'. *Palaeogeography, Palaeoclimatology, Palaeoecology, 154*(3), 161-178. https://doi.org/10.1016/S0031-0182(99)00109-1

Dooley, T. P., & Schreurs, G. (2012). Analogue modelling of intraplate strike-slip tectonics: A review and new experimental results. *Tectonophysics, 574-575*, 1-71. https://doi.org/10.1016/j.tecto.2012.05.030

Echeverria, A., Khazaradze, G., Asensio, E., Gárate, J., Dávila, J. M., & Suriñach, E. (2013). Crustal deformation in eastern Betics from CuaTeNeo GPS network. *Tectonophysics, 608*, 600-612. https://doi.org/10.1016/j.tecto.2013.08.020

Egan, S. S., Buddin, T. S., Kane, S. J., & Williams, G. D. (1997). Three-dimensional modelling and visualisation in structural geology: new techniques for the restoration and balancing of volumes. In *Proceedings of the 1996 Geoscience Information Group Conference on Geological Visualisation. Electronic Geology Special Volume* (Vol. 1, pp. 67-82).

Egan, S. S., Kane, S., Buddin, T. S., Williams, G. D., & Hodgetts, D. (1999). Computer modelling and visualisation of the structural deformation caused by movement along geological faults. *Computers & Geosciences, 25*(3), 283-297. https://doi.org/10.1016/S0098-3004(98)00125-3

Erslev, E. A. (1991). Trishear fault-propagation folding. *Geology*, *19*(6), 617-620.

Faure-Walker, J. P., Roberts, G. P., Cowie, P. A., Papanikolaou, I. D., Sammonds, P. R., Michetti, A. M., & Phillips, R. J. (2009). Horizontal strain-rates and throw-rates across breached relay zones, central Italy: Implications for the preservation of throw deficits at points of normal fault linkage. *Journal of Structural Geology*, *31*(10), 1145-1160. https://doi.org/10.1016/j.jsg.2009.06.011

Ferrater, M., Ortuño, M., Masana, E., Martínez-Díaz, J. J., Pallàs, R., Perea, H., … Arrowsmith, R. (2017). Lateral slip rate of Alhama de Murcia fault (SE Iberian Peninsula) based on a morphotectonic analysis: Comparison with paleoseismological data. *Quaternary International*, *451*, 87-100. https://doi.org/10.1016/j.quaint.2017.02.018

Ferrater, M., Ortuño, M., Masana, E., Pallàs, R., Perea, H., Baize, S., … Rhodes, E. J. (2016). Refining seismic parameters in low seismicity areas by 3D trenching: The Alhama de Murcia fault, SE Iberia. *Tectonophysics*, *680*, 122-128. https://doi.org/10.1016/j.tecto.2016.05.020

Fúster, J. M. & Gastesi, P. (1964). Estudio petrológico de las rocas lamproíticas de Barqueros (prov. de Murcia). *Estudios Geológicos*, *20*, 299-314.

Garcés, M., Krijgsman, W., & Agusti, J. (2001). Chronostratigraphic framework and evolution of the Fortuna basin (Eastern Betics) since the Late Miocene. *Basin Research*, *13*(2), 199-216. https://doi.org/10.1046/j.1365-2117.2001.00144.x

Garcés, M., Krijgsman, W., & Agustí, J. (1998). Chronology of the late Turolian deposits of the Fortuna basin (SE Spain): implications for the Messinian evolution of the eastern Betics. *Earth and Planetary Science Letters, 163*(1-4), 69-81. https://doi.org/10.1016/S0012-821X(98)00176-9

García-Dueñas, V., Balanyá, J. C., & Martínez-Martínez, J. M. (1992). Miocene extensional detachments in the outcropping basement of the northern Alboran Basin (Betics) and their tectonic implications. *Geo-Marine Letters*, *12*(2-3), 88-95. https://doi.org/10.1007/BF02084917

García-Mayordomo, J. (2005). Caracterización y Análisis de la Peligrosidad Sísmica en el Sureste de España (Doctoral dissertation). Universidad Complutense de Madrid, Madrid.

Geiser, J., Geiser, P. A., Kligfield, R., Ratliff, R., & Rowan, M. (1988). New Applications of Computer-Based Section Construction: Strain Analysis, Local Balancing, and Subsurface Fault Prediction. *The Mountain Geologist, 25*(2), 47-59.

Giba, M., Walsh, J. J., & Nicol, A. (2012). Segmentation and growth of an obliquely reactivated normal fault. *Journal of Structural Geology, 39*, 253-267. https://doi.org/10.1016/j.jsg.2012.01.004

Gibbs, A. D. (1983). Balanced cross-section construction from seismic sections in areas of extensional tectonics. *Journal of Structural Geology, 5*(2), 153-160. https://doi.org/10.1016/0191-8141(83)90040-8

Groshong, R. H. (1989). Half-graben structures: Balanced models of extensional fault-bend folds. *Geological Society of America Bulletin, 101*(1), 96-105. https://doi.org/10.1130/0016-7606(1989)101<0096:HGSBMO>2.3.CO;2

Groshong, R. H., Bond, C., Gibbs, A., Ratliff, R., & Wiltschko, D. V. (2012). Preface: Structural balancing at the start of the 21st century: 100 years since Chamberlin. *Journal of Structural Geology, 41*, 1-5. https://doi.org/10.1016/j.jsg.2012.03.010

Instituto Geográfico Nacional, IGN (2018). The Spanish seismic catalogue. IGN-Instituto Geográfico Nacional. Catálogo Sísmico Nacional. http://www.ign.es Last Accessed December 2018.

Instituto Geológico y Minero de España - IGME. (1972a). *Mapa Geológico de España a escala 1:50.000 (2a Serie)*. En MAGNA *Hoja 933 (Alcantarilla)*. IGME.

Instituto Geológico y Minero de España - IGME. (1972b). *Mapa Geológico de España a escala 1:50.000 (2a Serie)*. En Serie MAGNA *Hoja 912 (Mula)*. IGME.

Instituto Geológico y Minero de España - IGME. (2004). *Mapa Geológico Digital de España (Región de Murcia) (MGD50)*. IGME.

Instituto Geológico y Minero de España, IGME (2015). QAFI v.3: Quaternary Active Faults Database of Iberia. http://info.igme.es/QAFI. Last accessed 4th October 2018.

Instituto Geológico y Minero de España, IGME (2018). SIGEOF – Sistema de Información Geográfica – Geophysical Information System. Instituto Geológico y Minero de España (IGME). Available in: http://info.igme.es/SIGEOF/ Last accessed May 2018.

Krijgsman, W., Garcés, M., Agustí, J., Raffi, I., Taberner, C., & Zachariasse, W. J. (2000). The 'Tortonian salinity crisis' of the eastern Betics (Spain). *Earth and Planetary Science Letters, 181*(4), 497-511. https://doi.org/10.1016/S0012-821X(00)00224-7

Krijgsman, W., Leewis, M. E., Garcés, M., Kouwenhoven, T. J., Kuiper, K. F., & Sierro, F. J. (2006). Tectonic control for evaporite formation in the Eastern Betics (Tortonian; Spain). *The Messinian Salinity Crisis Revisited*, 188-189, 155-170. https://doi.org/10.1016/j.sedgeo.2006.03.003

Krishna, K. S., Bull, J. M., & Scrutton, R. A. (2009). Early (pre–8 Ma) fault activity and temporal strain accumulation in the central Indian Ocean. *Geology, 37*(3), 227-230. https://doi.org/10.1130/G25265A.1

Kuiper, K. F., Krijgsman, W., Garcés, M., & Wijbrans, J. R. (2006). Revised isotopic (40Ar/39Ar) age for the lamproite volcano of Cabezos Negros, Fortuna Basin (Eastern Betics, SE Spain). *Palaeogeography, Palaeoclimatology, Palaeoecology, 238*(1-4), 53-63. https://doi.org/10.1016/j.palaeo.2006.03.017

Lancis, C., Tent-Manclús, J.-E., Soria, J.-M., Caracuel, J.-E., Corbí, H., Dinarès-Turell, J., … Yébenes, A. (2010). Nannoplankton biostratigraphic calibration of the evaporitic events in the Neogene Fortuna Basin (SE Spain). *Geobios, 43*(2), 201-217. https://doi.org/10.1016/j.geobios.2009.09.007

Litchfield, N. J. (2001). The Titri Fault System: Quaternary-active faults near the leading edge of the Otago reverse fault province. *New Zealand Journal of Geology and Geophysics, 44*(4), 517-534. https://doi.org/10.1080/00288306.2001.9514953

Loiseau, J., Ott d'Estevou, P., & Montenat, C. (1990). Le secteur d'Archena−Mula. In *Documents et Travaux de l'IGAL* (Vol. 12, pp. 287-301).

Lonergan, L. & Schreiber, B. (1993). Proximal deposits at a fault-controlled basin margin, Upper Miocene, SE Spain. *Journal of The Geological Society, 150*, 719-727. https://doi.org/10.1144/gsjgs.150.4.0719

López-Comino, J.-Á., Mancilla, F. de L., Morales, J., & Stich, D. (2012). Rupture directivity of the 2011, Mw 5.2 Lorca earthquake (Spain). *Geophysical Research Letters, 39*(3), L03301. https://doi.org/10.1029/2011GL050498

López-Mir, B., Anton Muñoz, J., & García Senz, J. (2014). Restoration of basins driven by extension and salt tectonics: Example from the Cotiella Basin in the central Pyrenees. *Journal of Structural Geology, 69*, 147-162. https://doi.org/10.1016/j.jsg.2014.09.022

Lukowski, P., Wernli, R., & Poisson, A. (1988). New stratigraphical data concerning the late Miocene of the Fortuna basin, Murcia, Spain, showing the importance of the Messinian. *C. R. Acad. Sci. Paris, 307*, 941-947.

Martín-Banda, R., García-Mayordomo, J., Insua-Arévalo, J. M., Salazar, Á. E., Rodríguez-Escudero, E., Álvarez-Gómez, J. A., … Herrero, M. J. (2015). New insights on the seismogenic potential of the Eastern Betic Shear Zone (SE Iberia): Quaternary activity and paleoseismicity of the SW segment of the Carrascoy Fault Zone: the SW segment of the Carrascoy Fault. *Tectonics, 35*(1), 55-75. https://doi.org/10.1002/2015TC003997

Martínez del Olmo, W., Klimowitz, J., & Hernández, E. (2010). El despegue extensional mioceno de la zona de falla de Alhama de Murcia. *Boletín Geológico y Minero, 117*(3), 363-377.

Martínez-Díaz, J. J. (1998). *Neotectonica y Tectonica Activa del oeste de Murcia y sur de Almeria (Cordillera Betica)* (Doctoral Dissertation). Universidad Complutense Madrid, Madrid.

Martínez-Díaz, J. J., Bejar-Pizarro, M., Álvarez-Gómez, J. A., de Lis Mancilla, F., Stich, D., Herrera, G., & Morales, J. (2012a). Tectonic and seismic implications of an intersegment rupture: The damaging May 11th 2011 Mw 5.2 Lorca, Spain, earthquake. *Tectonophysics, 546*, 28-37.

Martínez-Díaz, J. J., Masana, E., & Ortuño, M. (2012b). Active tectonics of the Alhama de Murcia fault, Betic Cordillera, Spain. *Journal of Iberian Geology, 38*(1). https://doi.org/10.5209/rev_JIGE.2012.v38.n1.39218

Martínez-Díaz, J. J., Masana, E., Hernández-Enrile, J. L., & Santanach, P. (2003). Effects of repeated paleoeartquakes on the Alhama de Murcia fault (Betic Cordillera, Spain) on the Quaternary evolution of an alluvial fan system. *Annals of Geophysics, 46*(5), 775-792.

Martínez-Martínez, J. M., & Azañón, J. M. (1997). Mode of extensional tectonics in the southeastern Betics (SE Spain): Implications for the tectonic evolution of the peri-Alborán orogenic system. *Tectonics, 16*(2), 205-225. https://doi.org/10.1029/97TC00157

Masana, E., Martínez-Díaz, J. J., Hernández-Enrile, J. L., & Santanach, P. (2004). The Alhama de Murcia fault (SE Spain), a seismogenic fault in a diffuse plate boundary: Seismotectonic implications for the Ibero-Magrebian region. *Journal of Geophysical Research: Solid Earth, 109*(B1). https://doi.org/10.1029/2002JB002359

McClay, K. R. (1989). Analogue models of inversion tectonics. *Geological Society, London, Special Publications, 44*(1), 41-59. https://doi.org/10.1144/GSL.SP.1989.044.01.04

McClay, K. R. (1995). The geometries and kinematics of inverted fault systems: a review of analogue model studies. *Geological Society, London, Special Publications, 88*(1), 97-118. https://doi.org/10.1144/GSL.SP.1995.088.01.07

Meijninger, B. M. L. (2006). *Late-orogenic extension and strike-slip deformation in the Neogene of southeastern Spain* (Doctoral dissertation). Utrecht University.

Meijninger, B. M. L., & Vissers, R. L. M. (2006). Miocene extensional basin development in the Betic Cordillera, SE Spain revealed through analysis of the Alhama de Murcia and Crevillente Faults: Miocene extensional basin development in the Betic Cordillera. *Basin Research, 18*(4), 547-571. https://doi.org/10.1111/j.1365-2117.2006.00308.x

Mitra, S., & Namson, J. S. (1989). Equal-area balancing. *American Journal of Science, 289*(5), 563-599. https://doi.org/10.2475/ajs.289.5.563

Montenat, C. (1973). *Les formations neogènes et quaternaires du levant espagnol: Provinces d'Alicante et de Murcia* (Doctoral dissertation). Université de Paris Sud, Centre d'Orsay.

Montenat, C. & Ott d'Estevou, P. (1999). The diversity of late Neogene sedimentary basins generated by wrench faulting in the Eastern Betic Cordillera, SE Spain. *Journal of Petroleum Geology, 22*(1), 61-80. https://doi.org/10.1111/j.1747-5457.1999.tb00459.x

Montenat, C., Ott d'Estevou, P. & Masse, P. (1987). Tectonic sedimentary character of the Betic Neogene basins evolving in a crustal transcurrent shear zone (SE Spain). *Bull. Centres Rech. Explor-Prod. Elf-Aquitaine, 11*, 1-22.

Montenat, C., Ott d'Estevou, P., & Coppier, G. (1990). Les bassins néogènes entre Alicante et Cartagena. In *Documents et Travaux de l'IGAL* (Vol. 12, pp. 313–368).

Montenat, C., Thaler, L., & Van Couvering, J. (1975). La faune de rongeurs de Librilla. Corrélations avec les formations marines du Miocène terminal et les datations radiométriques du volcanisme de Barqueros (Province de Murcia, Espagne méridionale). *C. R. Acad. Sci. Paris, 281*, 519-522.

Müller, D. W. & Hsü, K. J. (1987). Event stratigraphy and paleoceanography in the Fortuna Basin (southeast Spain): A scenario for the Messinian salinity crisis. *Paleoceanography, 2*(6), 679-696. https://doi.org/10.1029/PA002i006p00679

Nixon, C. W., Sanderson, D. J., Dee, S. J., Bull, J. M., Humphreys, R. J., & Swanson, M. H. (2014). Fault interactions and reactivation within a normal-fault network at Milne Point, Alaska. *AAPG Bulletin, 98*(10), 2081-2107. https://doi.org/10.1306/04301413177

Nocquet, J.-M. (2012). Present-day kinematics of the Mediterranean: A comprehensive overview of GPS results. *Tectonophysics, 579*, 220-242. https://doi.org/10.1016/j.tecto.2012.03.037

Ortí, F., Veigas, J. G., Ortiz, L. R., Rouchy, J. M., Urpinell, M. I., Torrente, D. G., & Pous, E. P. (1993). Correlación litoestratigráfica de las evaporitas messinienses en las cuencas de Lorca y Fortuna (Murcia). *Geogaceta, 14*, 98-101.

Ortuño, M., Masana, E., Garcia-Melendez, E., Martinez-Diaz, J., Stepancikova, P., Cunha, P. P., … Murray, A. S. (2012). An exceptionally long paleoseismic record of a slow-moving fault: The Alhama de Murcia fault (Eastern Betic shear zone, Spain). *Geological Society of America Bulletin, 124*(9-10), 1474-1494. https://doi.org/10.1130/B30558.1

Playà, E., Ortí, F., & Rosell, L. (2000). Marine to non-marine sedimentation in the upper Miocene evaporites of the Eastern Betics, SE Spain: Sedimentological and geochemical evidence. *Sedimentary Geology, 133*(1-2), 135-166. https://doi.org/10.1016/S0037-0738(00)00033-6

Reilinger, R., & McClusky, S. (2011). Nubia–Arabia–Eurasia plate motions and the dynamics of Mediterranean and Middle East tectonics. *Geophysical Journal International, 186*(3), 971-979. https://doi.org/10.1111/j.1365-246X.2011.05133.x

Roberts, G. P., & Michetti, A. M. (2004). Spatial and temporal variations in growth rates along active normal fault systems: an example from The Lazio–Abruzzo Apennines, central Italy. *Journal of Structural Geology, 26*(2), 339-376. https://doi.org/10.1016/S0191-8141(03)00103-2

Rodríguez-Fernández, J., Azor, A., & Azañón, J. M. (2012). The Betic Intramontane Basins (SE Spain): Stratigraphy, Subsidence, and Tectonic History. In C. Busby, A. Azor (Eds.), *Tectonics of Sedimentary Basins* (pp. 461-479). https://doi.org/10.1002/9781444347166.ch23

Rotevatn, A., & Peacock, D. C. P. (2018). Strike-slip reactivation of segmented normal faults: Implications for basin structure and fluid flow. *Basin Research, 30*(6), 1264-1279. https://doi.org/10.1111/bre.12303

Santisteban, C. & Taberner, C. (1983). Shallow marine and continental conglomerates derived from coral reef complexes after desiccation of a deep marine basin: the Tortonian-Messinian deposits of the Fortuna Basin, SE Spain. *Journal of the Geological Society, 140*(3), 401-411. https://doi.org/10.1144/gsjgs.140.3.0401

Sanz de Galdeano, C. (1990). Geologic evolution of the Betic Cordilleras in the Western Mediterranean, Miocene to the present. *Tectonophysics, 172*(1-2), 107-119.

Sanz de Galdeano, C., López-Garrido, A. C., & García-Tortosa, F. J. (1998). Nuevos datos para la estimación de los valores de levantamiento desde el Tortoniense Superior a la actualidad en la parte centrooccidental de la Sierra de Carrascoy (provincia de Murcia). *Geogaceta, 142*, 139-142.

Scholz, C. H., & Cowie, P. A. (1990). Determination of total strain from faulting using slip measurements. *Nature, 346*(6287), 837-839. https://doi.org/10.1038/346837a0

Serpelloni, E., Vannucci, G., Pondrelli, S., Argnani, A., Casula, G., Anzidei, M., … Gasperini, P. (2007). Kinematics of the Western Africa-Eurasia plate boundary from focal mechanisms and GPS data. *Geophysical Journal International, 169*(3), 1180-1200. https://doi.org/10.1111/j.1365-246X.2007.03367.x

Sibson, R. H. (2009). Rupturing in overpressured crust during compressional inversion—the case from NE Honshu, Japan. *Tectonophysics, 473*(3-4), 404-416. https://doi.org/10.1016/j.tecto.2009.03.016

Sibson, R. H., & Ghisetti, F. C. (2010). Characterising the Seismic Potential of Compressional Inversion Structures, NW South Island. *Earthquake Commission, EQC Project, 8*(547), 38.

Silva, P. G., Goy, J. L., Zazo, C., & Bardají, T. (2003). Fault-generated mountain fronts in southeast Spain: geomorphologic assessment of tectonic and seismic activity. *Geomorphology, 50*(1-3), 203-225. https://doi.org/10.1016/S0169-555X(02)00215-5

Tent-Manclús, J. E., Soria, J. M., Estévez, A., Lancis, C., Caracuel, J. E., Dinarès-Turell, J. & Yébenes, A. (2008). The Tortonian salinity crisis in the Fortuna Basin (southeastern Spain): Stratigraphic record, tectonic scenario and chronostratigraphy. *Comptes Rendus Geoscience, 340*(7), 474-481. https://doi.org/10.1016/j.crte.2008.05.003

Vissers, R. L. M., Platt, J. P., & van der Wal, D. (1995). Late orogenic extension of the Betic Cordillera and the Alboran Domain: A lithospheric view. *Tectonics, 14*(4), 786-803. https://doi.org/10.1029/95TC00086

Walsh, J. J., & Watterson, J. (1989). Displacement gradients on fault surfaces. *Journal of Structural Geology, 11*(3), 307-316. https://doi.org/10.1016/0191-8141(89)90070-9

Watkins, H., Bond, C. E., & Butler, R. W. H. (2014). Identifying multiple detachment horizons and an evolving thrust history through cross-section restoration and appraisal in the Moine Thrust Belt, NW Scotland. *Journal of Structural Geology, 66*, 1-10. https://doi.org/10.1016/j.jsg.2014.05.001

Watkins, H., Butler, R. W. H., & Bond, C. E. (2017). Using laterally compatible cross sections to infer fault growth and linkage models in foreland thrust belts. *Journal of Structural Geology, 96*, 102-117. https://doi.org/10.1016/j.jsg.2017.01.010

White, N., & Yielding, G. (1991). Calculating normal fault geometries at depth: theory and examples. *Geological Society, London, Special Publications, 56*(1), 251-260. https://doi.org/10.1144/GSL.SP.1991.056.01.18

Youngs, R. R., & Coppersmith, K. J. (1985). Implications of fault slip rates and earthquake recurrence models to probabilistic seismic hazard estimates. *Bulletin of the Seismological Society of America, 75*(4), 939-964.

Zechar, J. D., & Frankel, K. L. (2009). Incorporating and reporting uncertainties in fault slip rates. *Journal of Geophysical Research, 114*(B12). https://doi.org/10.1029/2009JB006325

Ziesch, J., Tanner, D. C., & Krawczyk, C. M. (2014). Strain Associated with the Fault-Parallel Flow Algorithm During Kinematic Fault Displacement. *Mathematical Geosciences, 46*(1), 59-73. https://doi.org/10.1007/s11004-013-9464-3

Table and figure captions

Table 1. Dip-slip and heave results in meters for each restored profile. The quantification of two steps of restoration are shown: restoration of the units Intra-Messinian 1 and 2 and restoration of the Tortonian top horizon. The latter represents cumulative displacement and is used to estimate the rates. A ±3.4 m uncertainty is considered for each measure. (*)Total dip-slip and total heave refer to the intra-Messinian markers restoration.

	Dip-Slip (m)		**Heave (m)**	
	Intra-Messinian 1 – 2	*Tortonian top horizon*	*Intra-Messinian 1 – 2*	*Tortonian top horizon*
S-84-52	699	**1227**	377	**597**
S-85-92	284	**673**	143	**319**
S-84-56	162	**162***	92	**92***

Table 2. Dip-slip rates and shortening rates, in mm/yr. The results are reported following the probabilistic format suggested by Zechar and Frankel (2009). A range of ages between the last 4.8 and 7.6 Ma has been considered as a boxcar distribution, with a Gaussian displacement uncertainty of ±3.4 m. The probability distributions are available in the Supporting information.

	Dip-slip rate (mm/yr)			**Shortening rate (mm/yr)**		
Profile – sector	**Median**	***68.27% Interval***	***95.45% Interval***	**Median**	***68.27% Interval***	***95.45% Interval***
S-84-52 – Librilla sector	**0.198**	+0.036/-0.027	+0.054/-0.035	**0.096**	+0.018/-0.013	+0.027/-0.017
S-85-92 – Librilla sector	**0.109**	+0.020/-0.015	+0.030/-0.019	**0.051**	+0.009/-0.007	+0.014/-0.009
S-84-56 – Alcantarilla sector	**0.026**	+0.005/-0.004	+0.007/-0.005	**0.015**	+0.003/-0.002	+0.004/-0.003

Table 3. Strike-slip rates and net-slip rates, in mm/yr. The results are reported following the probabilistic format suggested by Zechar and Frankel (2009). A range of ages between the

last 4.8 and 7.6 Ma has been defined, using all convergence vectors from the GPS sites of CuaTeNeo network, modified from Echeverría et al. (2013) in our work. The probability distributions are available in the Supporting information.

	Strike-slip rate (mm/yr)			**Net – slip rate (mm/yr)**		
Profile – sector *all GPS convergence vectors considered*	**Median**	***68.27% Interval***	***95.45% Interval***	**Median**	***68.27% Interval***	***95.45% Interval***
S-84-52 – Librilla sector	**0.232**	+0.114/-0.112	+0.208/-0.156	**0.300**	+0.102/-0.092	+0.195/-0.129
S-85-92 – Librilla sector	**0.126**	+0.062/-0.061	+0.113/-0.085	**0.163**	+0.055/-0.050	+0.106/-0.070
S-84-56 – Alcantarilla sector	**0.035**	+0.017/-0.017	+0.032/-0.024	**0.046**	+0.015/-0.014	+0.030/-0.020

Table 4. Net-slip rates, in mm/yr, assuming the best-fit orientations of the slip vector (last 4.8 – 7.6 Ma). We have given weight to a preferred range of net-slips, without excluding the absolute range of slip vectors. The results are shown following the probabilistic format suggested by Zechar and Frankel (2009). The probability distributions are available in the Supporting information.

	Net – slip rate (mm/yr)		
Profile – sector *preferred range of GPS convergence vectors*	**Median**	***68.27% Interval***	***95.45% Interval***
S-84-52 – Librilla sector	**0.323**	+0.091/-0.080	+0.178/-0.128
S-85-92 – Librilla sector	**0.176**	+0.049/-0.043	+0.097/-0.070
S-84-56 – Alcantarilla sector	**0.049**	+0.014/-0.012	+0.027/-0.019

Table 5. Summary of all the slip rates estimated, in mm/yr. The results are shown following the probabilistic format suggested by Zechar and Frankel (2009). The uncertainties are

equivalent to the 95.45% confidence interval. The probability distributions are available in the Supporting information.

		Shortening rate (mm/yr)		*Strike-slip rate (mm/yr)*		*Net-slip rate (mm/yr)*		*Age*	*Convergence vectors*
Alcantarilla sector	S-84-56	**0.015**	+0.004/-0.003	**0.035**	+0.032/-0.024	0.05	+0.02/-0.02	Last 5.3 – 7.6 Ma	best-fit
						0.05	+0.03/-0.02	Last 4.8 – 7.6 Ma	
						0.05	+0.03/-0.02		all
Librilla sector	S-85-92	**0.05**	+0.01/-0.01	**0.13**	+0.11/-0.09	0.17	+0.08/-0.06	Last 5.3 – 7.6 Ma	best-fit
						0.18	+0.10/-0.07	Last 4.8 – 7.6 Ma	
						0.16	+0.11/-0.07		all
	S-84-52	**0.10**	+0.03/-0.02	**0.23**	+0.21/-0.16	0.31	+0.15/-0.12	Last 5.3 – 7.6 Ma	best-fit
						0.32	+0.18/-0.13	Last 4.8 – 7.6 Ma	
						0.30	+0.20/-0.13		all
'La Muela' sector		*max. uplift rate (mm/yr)* 0.26 – 0.42						Last 4.8 – 7.6 Ma	

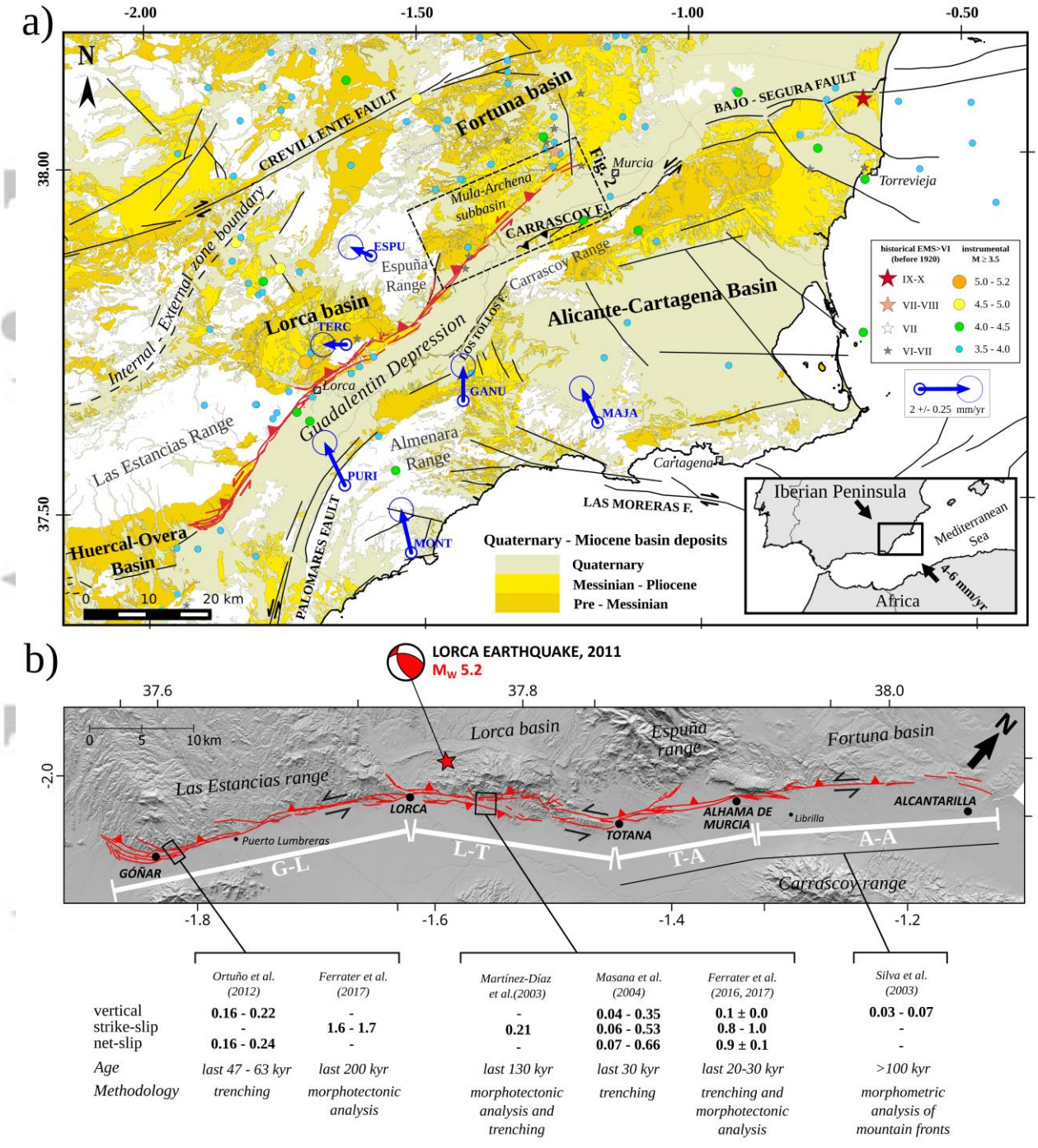

	Ortuño et al. (2012)	Ferrater et al. (2017)	Martínez-Díaz et al.(2003)	Masana et al. (2004)	Ferrater et al. (2016, 2017)	Silva et al. (2003)
vertical	**0.16 - 0.22**	-	-	**0.04 - 0.35**	**0.1 ± 0.0**	**0.03 - 0.07**
strike-slip	-	**1.6 - 1.7**	**0.21**	**0.06 - 0.53**	**0.8 - 1.0**	-
net-slip	**0.16 - 0.24**	-	-	**0.07 - 0.66**	**0.9 ± 0.1**	-
Age	*last 47 - 63 kyr*	*last 200 kyr*	*last 130 kyr*	*last 30 kyr*	*last 20-30 kyr*	*>100 kyr*
Methodology	*trenching*	*morphotectonic analysis*	*morphotectonic analysis and trenching*	*trenching*	*trenching and morphotectonic analysis*	*morphometric analysis of mountain fronts*

Figure 1. Geological and tectonic setting of the Eastern Betic Shear Zone (EBSZ). (**a**) Epicenter of instrumental earthquakes with magnitude M≥3.5 and historical earthquakes from the period before 1920 with intensity EMS>VI, data from the "Instituto Geográfico Nacional" - https://www.ign.es/web/ign/portal/sis-catalogo-terremotos. The blue arrows represent the CuaTeNeo GPS velocities in Western Europe reference frame (Echeverria et al., 2013) used in our research. Alhama de Murcia Fault (AMF) is represented in red. The geological map of the study area (Figure 2) is located in the inset. The lower right inset shows the regional location of the Eastern Betics and the main convergence direction. (**b**) Segmentation of the Alhama de Murcia Fault from Martínez-Díaz et al. (2012) and summary of available slip rates for the AMF (Martínez-Díaz et al., 2003; Silva et al., 2003; Masana et al., 2004; Ortuño et al., 2012; Ferrater et al., 2016, 2017). Fault traces from the Quaternary

Active Faults Database of Iberia v.3 (QAFI, IGME, 2015). The star represents the epicenter of the Lorca 2011 M_W 5.2 earthquake. The AMF sections defined by Martínez-Díaz et al., (2012) are: Góñar – Lorca (G-L), Lorca – Totana (L-T), Totana – Alhama de Murcia (T-A) y Alhama de Murcia – Alcantarilla (A-A).

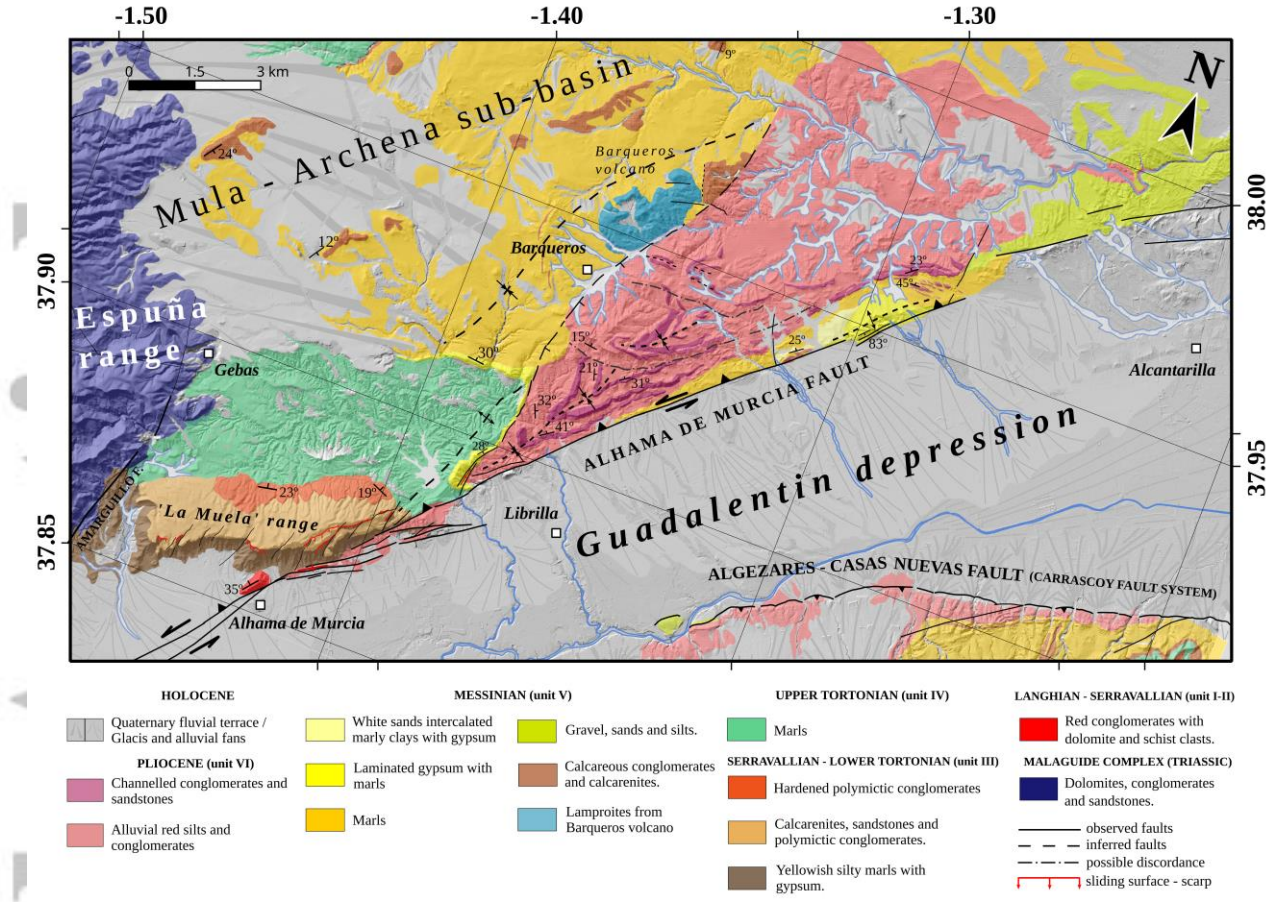

Figure 2. Geological map of the southwestern sector of the Fortuna Basin (Mula-Archena sub-basin), Alhama de Murcia-Alcantarilla section of the AMF and northern part of the Guadalentin depression, based on previous cartography (IGME, 1972a, 1972b, 2004), publications (e.g., Martínez-Díaz, 1998; Martínez-Díaz et al., 2012; Meijninger, 2006; Montenat et al., 1990) and fieldwork. Coordinate reference system: WGS84 ellipsoid.

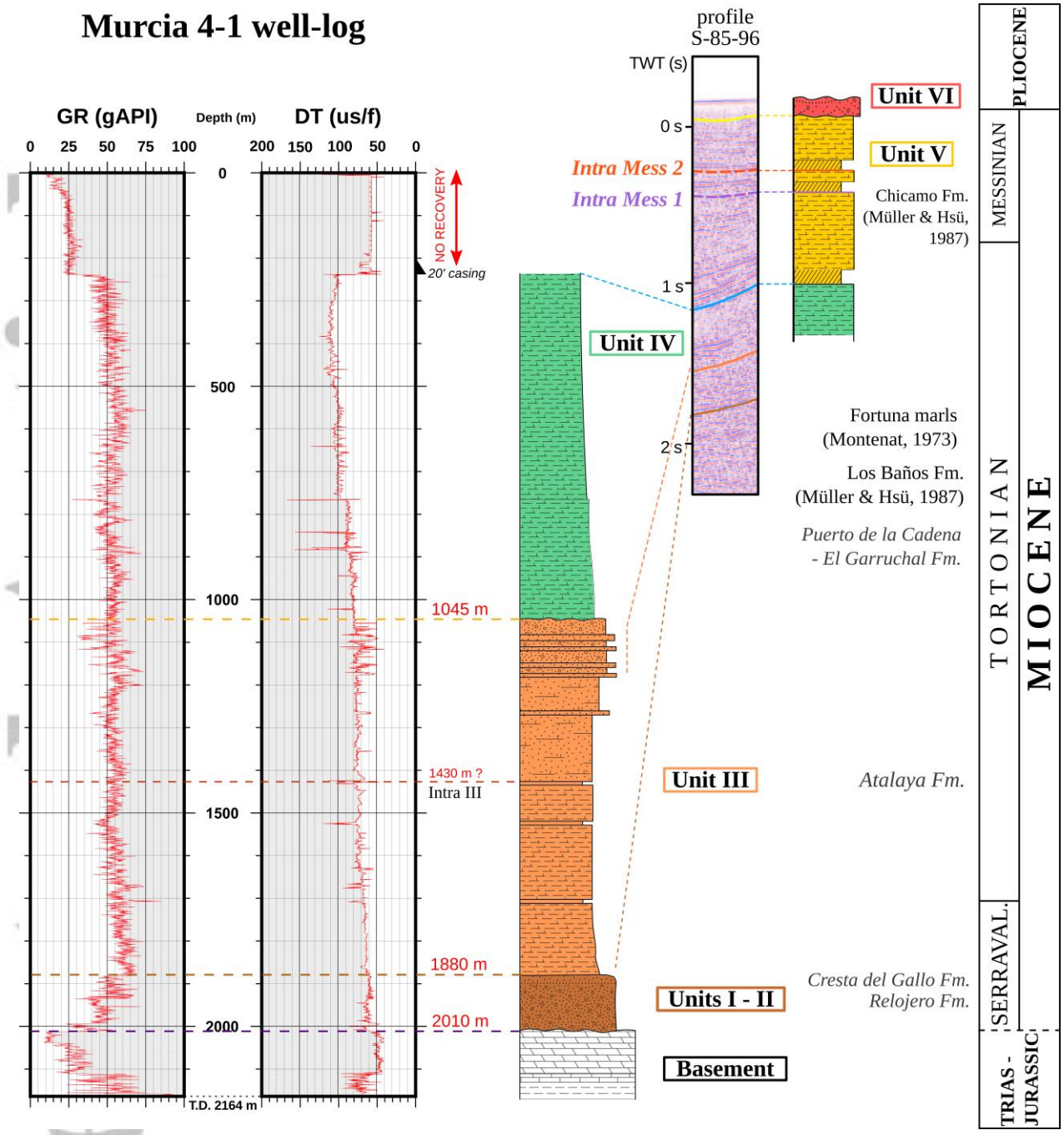

Figure 3. Correlation between the litostratigraphic units and well and seismic data. On the left, gamma-ray log (GR) and sonic log (DT) in measured depth from Murcia 4-1 well (IGME, 2018) used to better constrain the interpretation and correlate the stratigraphic units (in Roman numeral). Depths are in meters below the kelly bushing (KB). The logging record starts below 241 m. Red values along the right plot correspond to depths estimated for changes in the sequence, illustrated with a litostratigraphic column, in the center of the figure, with the main lithologies in each unit. Note that the correlation between the well-log and the stratigraphic column only covers the basement, units I-II, III and part of the unit IV. The upper part of the sequence is correlated with seismic data from the profile S-85-96 (see Fig. 4 and Supporting information). The rectangular inset shows partial seismic data in Two-way traveltime (TWT) from a position close to the Murcia 4-1 well and the main reflections and discontinuities used in the seismic interpretation conducted in the Mula-Archena sub-basin are represented. Note that the scales and units of measurement in the well-log, the schematic

column and the seismic section are not the same. Main ages and stratigraphic formations described in the region (IGME, 1972a, 1972b, 2004; Montenat, 1973; Müller and Hsü, 1987) are shown on the right for reference. T.D. = Total depth; Intra Mess 1, 2 = units Intra-Messinian 1 and 2; Intra III = internal discontinuity in Unit III.

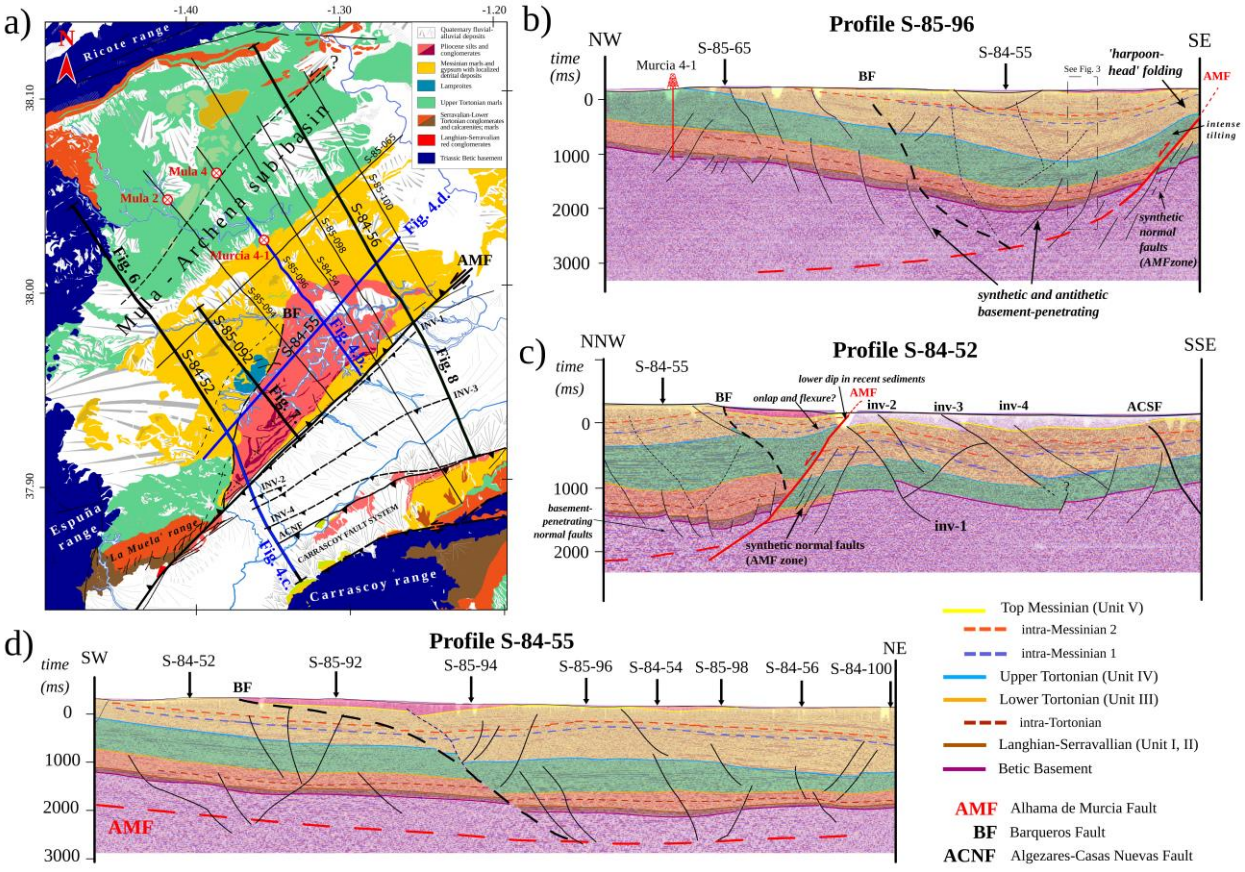

Figure 4. Interpretation of seismic reflection profiles from the Mula-Archena subbasin. (**a**) Regional map of the location of the profiles interpreted in our research. Blue lines are the profiles shown in this figure. Thick black lines represent the restored profiles shown in Figures 6, 7 and 8. The Murcia 4-1, Mula 2 and Mula 4 wells are represented with a red and white circle. The faults in the map are correlated with the structures interpreted in the profiles. (**b**), (**c**) and (**d**) show the interpretation of the profiles S-85-96, S-84-52 and S-84-55, respectively. The y-axis is in milliseconds (TWT). The intersections with other profiles are indicated with vertical arrows. The structural features described in the text are written in italics. The AMF trace with red broken line represents a low-angle normal fault interpreted by several authors (see Discussion). AMF = Alhama de Murcia fault; BF = Barqueros fault; ACSF = Algezares – Casas Nuevas fault; INV-(1-4) = inverse faults interpreted in the Guadalentín depression.

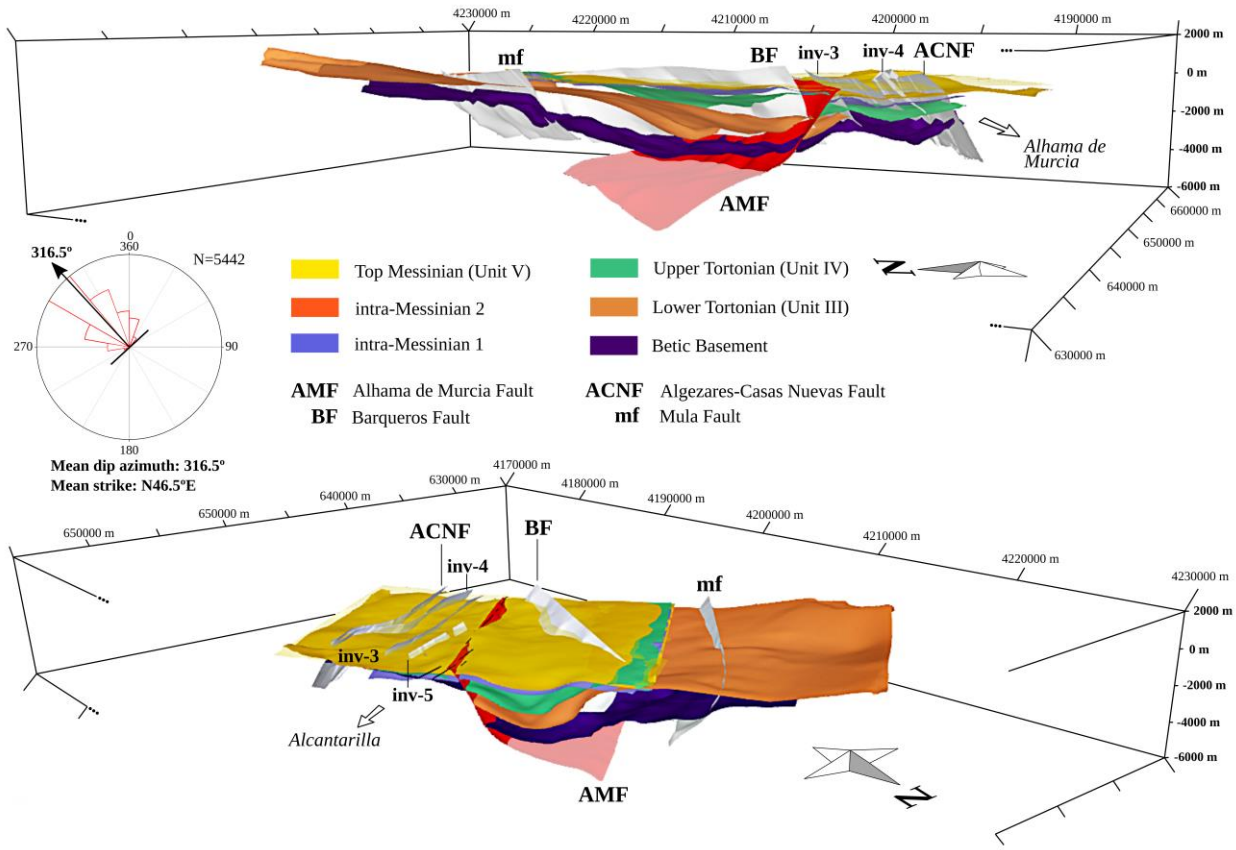

Figure 5. 3D geological model of the southwestern sector of the Fortuna Basin and northern part of the Guadalentin depression, based on the interpretation of seismic reflection profiles and well data. The model is shown from two points of view: above, from the NW; below, from the N-NE. The Alhama de Murcia fault plane considered in this work is highlighted in red. The shaded part displays the model of low-angle fault interpreted by several authors (see Discussion) and represented in Figure 4a, 4b and 4c with red broken lines. The mean dip direction (316.5º) is shown in a rose plot on the left. AMF = Alhama de Murcia fault; BF = Barqueros fault; ACSF = Algezares – Casas Nuevas fault; mf = Mula fault; INV-(3-5) = inverse faults interpreted in the Guadalentín depression. Coordinate reference system: ETRS89 / UTM zone 30N.

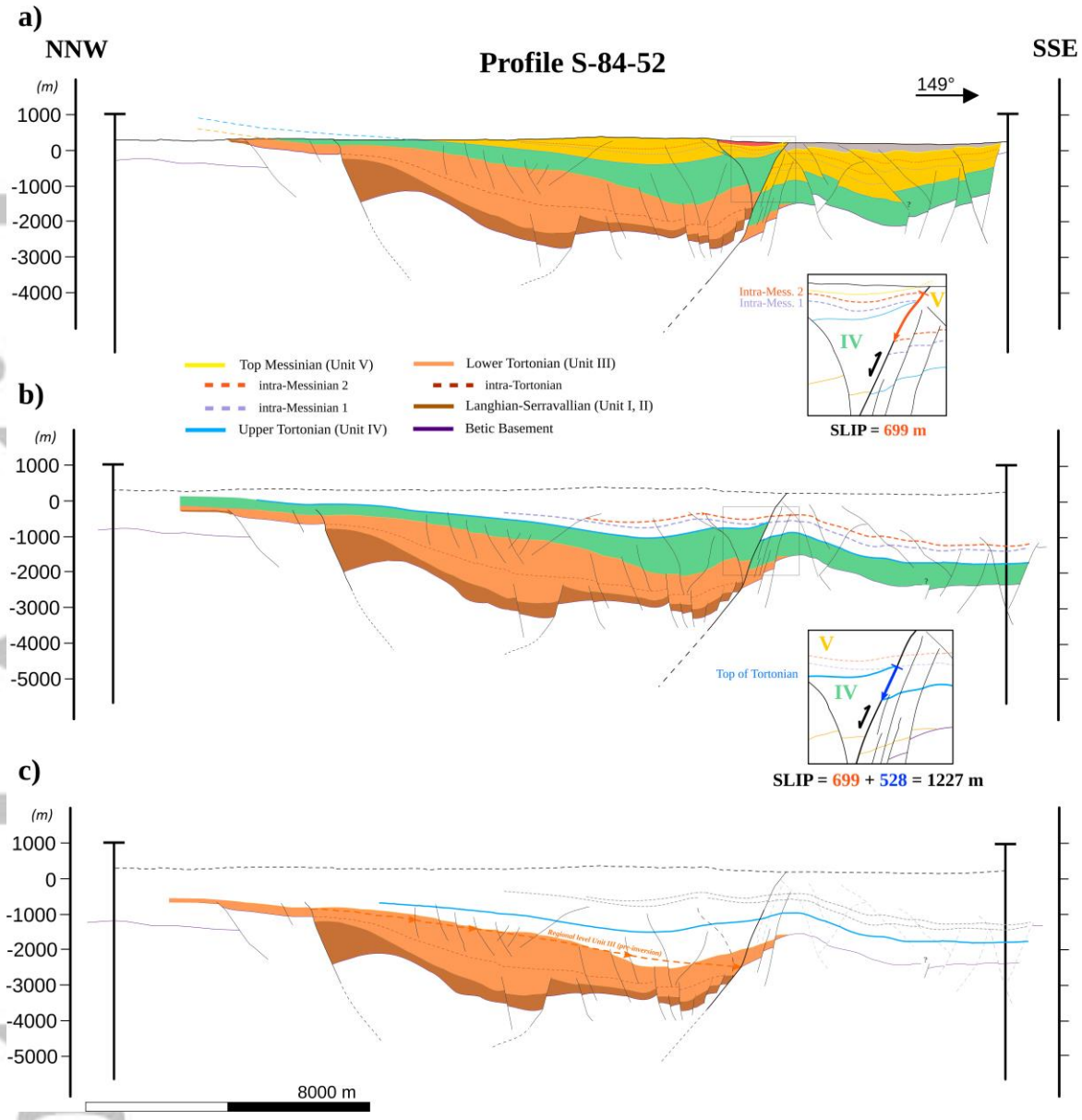

Figure 6. Restoration of the stratigraphic marker horizons in the profile S-84-52. The location of the seismic line is shown in Figure 4a. The Y-axis is in depth below sea level (meters). (**a**) Original interpretation based on seismic data. (**b**) Step corresponding to the restoration of the intra-Messinian markers (units Intra-Messinian 1 and 2). Before, the fault offsets in the Guadalentín depression and other minor faults in the basin have also been restored, but those steps are omitted in the figure. (**c**) Restoration of the Tortonian top horizon (between units IV and V). The detail restorations are displayed in the insets between the steps, with the measurement of the displacements estimated. In c) an estimation of the regional level of Unit III before the basin inversion is shown. This estimation has allowed to approximate a value of uplift for the sector of 'La Muela'. The rest of steps of restoration that affect the units III, II and the Basement are omitted in the figure because they are not involved in the estimation of recent slips.

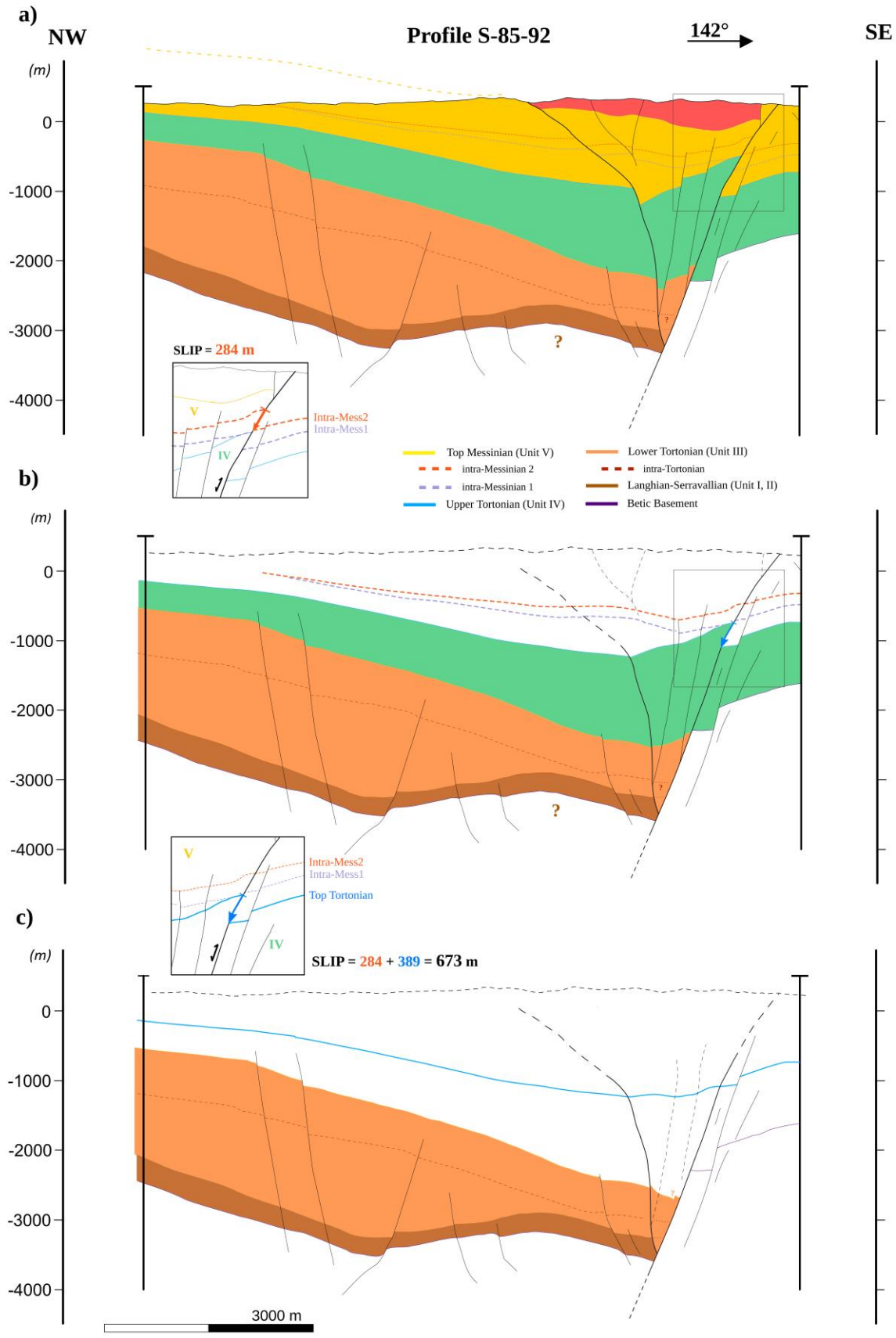

Figure 7. Restoration of the stratigraphic marker horizons in the profile S-85-92. The location of the seismic line is in Figure 4a. The Y-axis is in depth below sea level (meters).

(**a**) Original interpretation based on seismic data. (**b**) Step corresponding to the restoration of the intra-Messinian markers (units Intra-Messinian 1 and 2). Other minor offsets have also been restored, but those steps are omitted in the figure. (**c**) Restoration of the Tortonian top horizon (between units IV and V). The detail restorations are displayed in the insets between the steps, with the measurement of the displacements estimated.

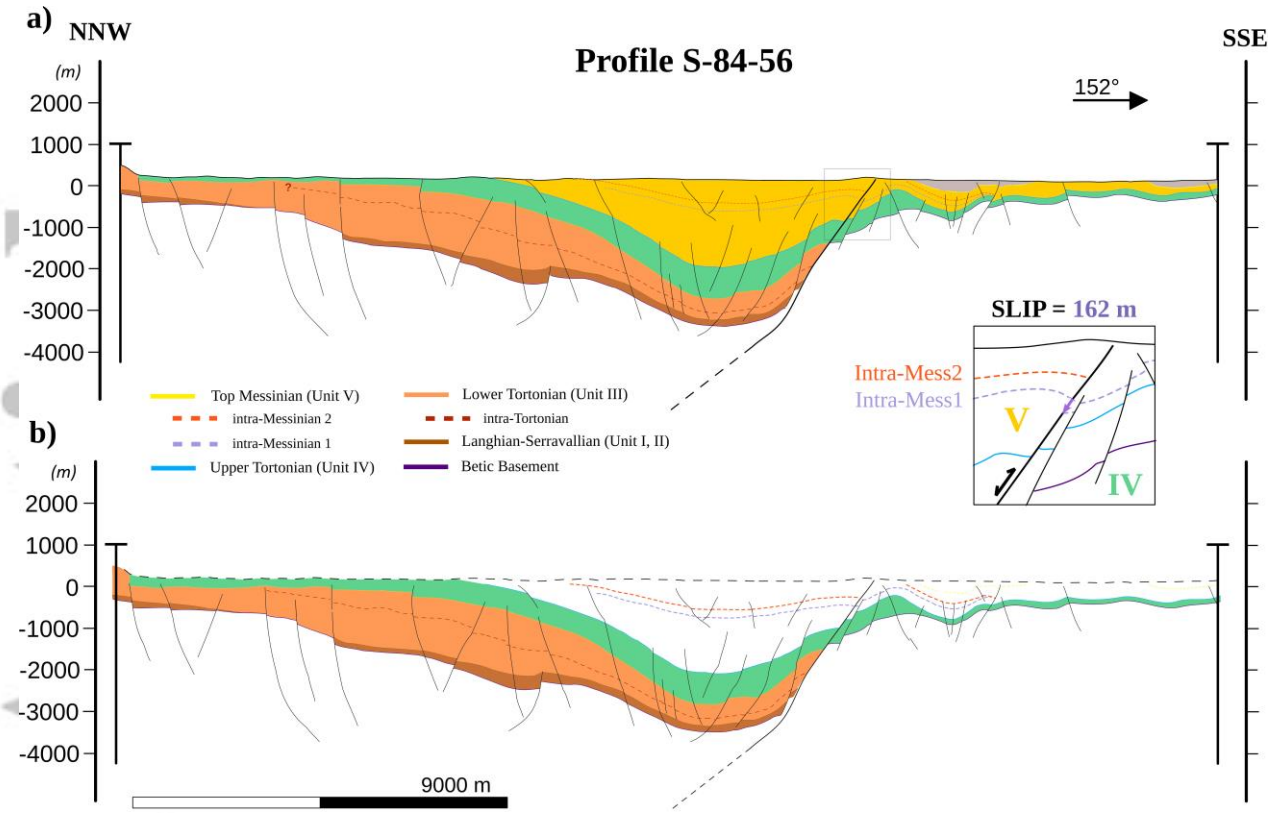

Figure 8. Restoration of the stratigraphic marker horizons in the profile S-84-56. The location of the profile is shown in Figure 4a. The Y-axis is in depth below sea level (meters). (**a**) Original interpretation based on seismic data. (**b**) Restoration of the intra-Messinian markers (units Intra-Messinian 1 and 2). Other minor offsets have also been restored, but the steps are omitted in the figure. The rest of steps of restoration that affect the units III, II and the Basement are omitted in the figure because they are not involved in the estimation of recent slips.

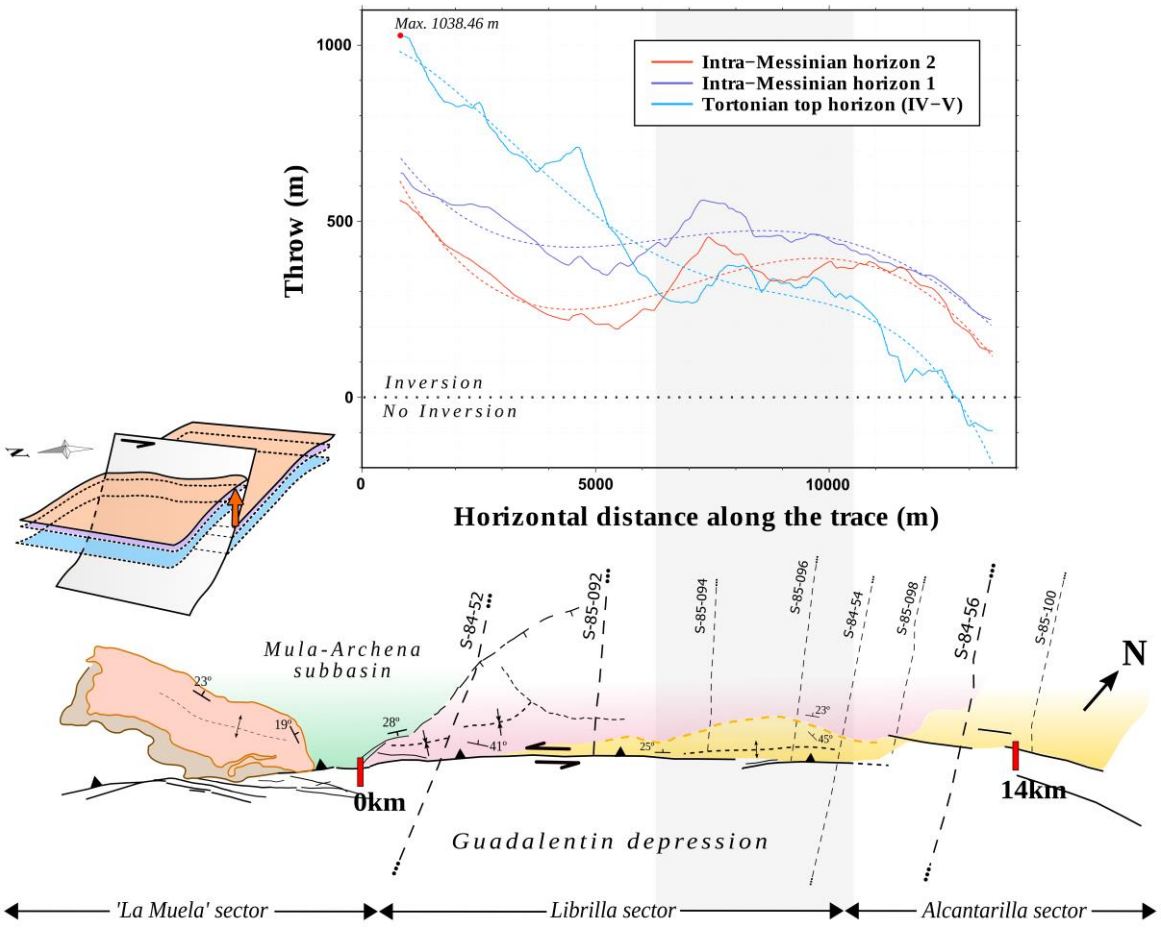

Figure 9. Throw distribution (in meters) along the fault trace in the northern termination of the AMF based on 3D vertical displacement analysis. The plot shows a decrease in vertical throw along the horizontal distance from SW to NE, with the exception of a zone at 6-11 km horizontal distance, with shading in the plot (see explanation in text). Positive values of throw concern the positive inversion and negative values imply low or even null slip. Dash lines represent the polynomial trend fitted to the data of each marker. Below, the position of the seismic profiles, faults and some structures regarding the graph are illustrated schematically. The omission of the first and last meters in the graph is due to artifacts observed in the edges of the 3D surfaces related to the interpolation method. On the left, a sketch of the 3D model illustrates the procedure.

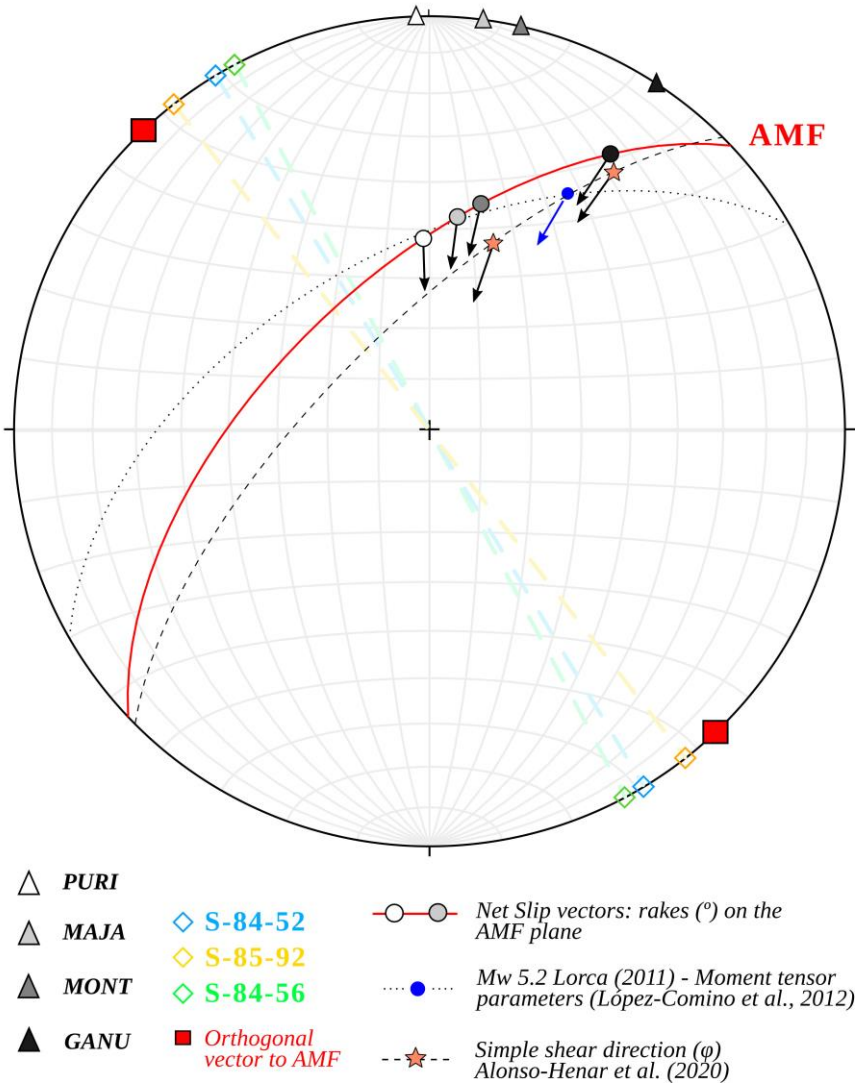

Figure 10. Orientations of net-slips estimated and other geological and seismological data analyzed. The grey-scale circles of the stereoplot represent the rake angles on the fault plane (in red) of the resulted net-slip vectors. These vectors are dependent on the local convergence vectors from the GPS sites represented with triangles (same grey-scale): PURI, MAJA, MONT and GANU. Local geodetic data have been modified from Echeverría et al. (2013), but considering the northern block of the AMF as fixed reference frame. The squares symbolize the azimuth of the restored profiles and the vector orthogonal to the fault (in the horizontal plane). Blue circle represents the slip vector rake of the focal mechanism for the Lorca 2011 M_W 5.2 earthquake (Lopez-Comino et al., 2012). The stars show the extreme obliquity angles of simple shear direction suggested by Alonso-Henar et al. (2020) in the Lorca-Totana section.

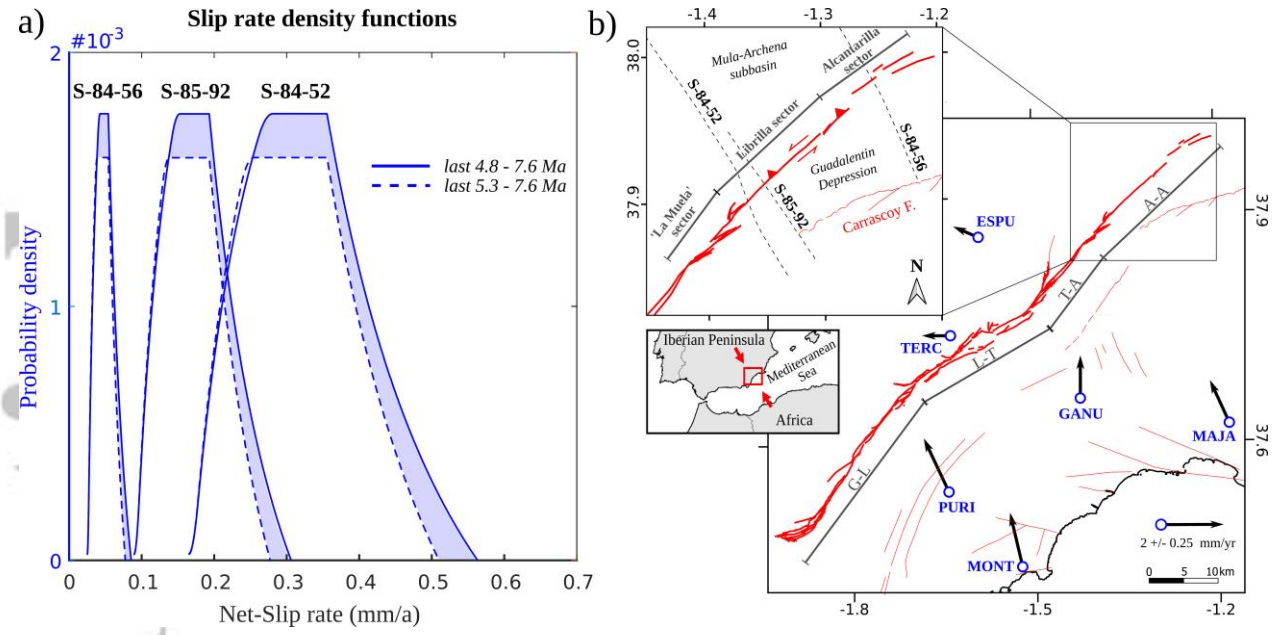

Figure 11. a) Net-slip rate probability distributions for the profiles S-84-56, S-85-92 and S-84-56, assuming the best-fit orientations of the slip vector and two different ranges of ages: for the last 4.8 – 7.6 Ma and for the last 5,3 – 7,6 Ma (in broken line). The estimations were done applying Zechar and Frankel (2009) density functions. Note that the median for the last 5.3 – 7.6 Ma does not differ significantly from the median for the last 4.8 – 7.6 Ma, although the uncertainties are smaller. b) Location map of the profiles and sectors analyzed in the Alhama de Murcia – Alcantarilla section. GPS sites and motion vectors are shown.